AN EVALUATION OF FERROUS IRON OXIDATION KINETICS IN A MULTIPLE ORIFICE SPRAY REACTOR

by

Daniel B. Klein

B.S., Towson University, 2000

M.S., Florida International University, 2003

Submitted to the Graduate Faculty of

School of Engineering in partial fulfillment

of the requirements for the degree of

M.S. Civil Engineering

University of Pittsburgh

2005

UNIVERSITY OF PITTSBURGH

SCHOOL OF ENGINEERING

This thesis was presented

by

Daniel B. Klein

It was defended on

March 21, 2005

and approved by

Dr. L. Casson, Associate Professor, Civil and Environmental Engineering

Dr. R. Quimpo, Professor, Civil and Environmental Engineering

Thesis Advisor: Dr. R. D. Neufeld, Professor, Civil and Environmental Engineering

AN EVALUATION OF FERROUS IRON OXIDATION KINETICS IN A MULTIPLE ORIFICE SPRAY REACTOR

Daniel B. Klein, M.S.

University of Pittsburgh, 2005

A bench scale experiment using a multiple orifice spray reactor was investigated as a potential remediation technology for the rapid oxidation of ferrous iron in acidic mine discharges. The multiple orifice spray reactor makes use of flow through multiple orifices to enhance aqueous aeration and oxidation rates. The reactor consists of two concentric cylinders, the inner cylinder having a series of orifices which act in a manner similar to a venturi. In this fashion neutralization and aeration are combined into a single step due to the aspiration of air as a result of a pressure gradient across the reactor which allows for the suction of an alkaline agent in to the reaction chamber.

Results show ferrous iron oxidation rates at pH values between 6 and 7 can be increased by four orders of magnitude as compared to theoretical oxidation rates. At an influent ferrous iron concentration of around 150 mg/L and pH of 6, the orifice spray reactor can achieve conversions to ferric iron of about 30% within one second.

TABLE OF CONTENTS

PREFACE x

1.0 PROBLEM STATEMENT 1

1.1 SURFACE WATER QUALITY STANDARD 2

2.0 LITERATURE REVIEW 4

2.1 ACID MINE DRAINAGE CHEMISTRY 4

2.2 IRON OXIDATION 6

2.2.1 Iron Dependent Model 6

2.2.2 Factors Affecting Iron Oxidation 7

2.2.3 Acid Mine Drainage Treatment 13

2.2.4 Passive Treatment 15

2.2.5 Active Treatment 15

2.2.5.1 In Line Aeration and Neutralization System (ILS) 16

2.2.5.2 Turbojett (TJ) 17

3.0 MATERIALS AND METHODS 21

3.1 BENCH SCALE SYSTEM 22

3.2 MINE WATER 26

3.3 SURROGATE AMD SOLUTION 27

3.4 OXYGEN TRANSFER RATES 28

3.5 FERROUS IRON OXIDATON RATES 29

4.0 RESULTS AND DISCUSSION 31

4.1 MOSR HYDRAULIC CHARACTERISTICS 31
4.2 OXYGEN TRANSFER CAPABILITIES 35
4.3 FERROUS IRON OXIDATION 41
4.3.1 Hydrolysis 41
4.3.2 Mine Water 43
4.3.3 Oxidation as a Function of Pressure 45
4.3.4 Oxidation as a Function of Time in MOSR Effluent 47
4.3.5 The Effect of Ferrous Concentration on Oxidation 51
4.4 NITROGEN EXPERIMENTS 54
4.5 IRON REMOVAL VERSUS OXIDATION 57
5.0 SUMMARY AND CONCLUSIONS 62
6.0 RECOMMENDATIONS FOR FUTURE WORK 65
APPENDIX A 69
EXPERIMENTAL DATA 69
BIBLIOGRAPHY 99

LIST OF TABLES

Table 1 EPA coal mining effluent water quality 3

Table 2 Residence times of the MOSR as a function of pressure..... 25

Table 3. Ferrous Iron Oxidation Test Procedure, ... 27

Table 4 Results of sulfite oxidation in the MOSR. P (psi) = 72, $[O_2]_t$ = 0mg/L. 38

Table 5 Results of hot peroxide titration on St. Michael's mine water sample..... 42

Table 6 Results of SO_3 oxidation in the presence of N_2 gas..... 55

Table 7 Results of ferrous iron oxidation in the presence of N_2 gas. Q = 0.7 gpm, P = 73 psi, T=22-27ºC..... 56

Table 8 Results of total iron concentrations of filtered MOSR effluents. Samples collected immediately exiting the MOSR. 59

Table A 1 St. Michaels's mine water experimental oxidation rate 69

Table A 2 Flow rate as a function of pressure in the MOSR experimental system..... 70

Table A 3 Data showing measurement of O_2 transfer at 70 psi..... 71

Table A 4 Second test on O_2 transfer at 70 psi 72

Table A 5 O_2 transfer using N_2 as the de - oxygenating agent 73

Table A 6 k_{La} measurements in the bulk liquid 74

Table A 7 Calibration curve for SO_4 measurements..... 75

Table A 8 Data showing D.O. concentrations versus time with and with out HCHO..... 76

Table A 9 Results of SO_3 oxidation tests conducted on the MOSR 77

Table A 10 Data for typical ferrous iron calibration curve..... 78

Table A 11 St. Michael's mine water oxidation tests..... 79

Table A 12 Condensed results of St. Michael's mine water tests 86

Table A 13 Comparison of MOSR oxidation rate to theory 87

Table A 14 Caustic addition as a function of flow rate 87

Table A 15 Ferrous iron oxidation tests as a function of pressure 88

Table A 16 Oxygen transfer tests as a function of pressure 91

Table A 17 Ferrous iron oxidation as a function of initial ferrous iron concentration 92

Table A 18 Data showing ferrous iron oxidation in MOSR effluent as a function of time 97

Table A 19 Ferrous iron oxidation as a function of time in control samples 98

LIST OF FIGURES

Figure 1 Ferrous and ferric iron solubility diagram 6

Figure 2 Two film theory of gas transfer, very slow or no chemical reaction 9

Figure 3 Two film theory, instantaneous reaction 12

Figure 4 Process flow diagram for AMD treatment 13

Figure 5 ILS cross section 16

Figure 6 TJ cross section 18

Figure 7 Experimental setup 22

Figure 8 MOSR cross section 23

Figure 9 Schematic showing sampling 29

Figure 10 Flow rate as a function of pressure. The max. pressure is 75 psi due to the physical limitations of the pump used (1gpm = 3.785 Lpm). 32

Figure 11 Images of the inner cylinder of the MOSR at various pressures. 33

Figure 12 Exit sprays of the MOSR at different pressures. 34

Figure 13 Oxygen transfer measurements of the MOSR at different operating pressures. T(ºC) = 23.5, $[O_2]_{sat}$=8.7 mg/L. 36

Figure 14 Mass transfer zones in the MOSR 40

Figure 15 Ferrous iron oxidation rates, theoretical and experimental. T(ºC) = 22 ºC, P(psi) = 70 ± 5 43

Figure 16 Ferrous iron oxidation as a function of pressure. $[Fe^{+2}]$ = 150 mg/L, pH = 8.8±0.5, NaOH flow rate = 150 mL/min. 45

Figure 17 Oxygen Transfer and iron oxidation as a function of pressure. K_La measured using a DO probe. $[Fe^{+2}]$ = 150 mg/L, pH = 8.8±0.5, NaOH flow rate = 150 mL/min. 46

Figure 18 Ferrous iron oxidation as a function of time, MOSR effluent and an aerated control sample 48

Figure 19 Dissolved oxygen and pH values as a function of time in the MOSR effluent bulk liquid 50

Figure 20 Zones of oxidation in the MOSR..... 51

Figure 21 Ferrous iron oxidation as a function of concentration. P(psi) = 70, NaOH = 0.015 eq/L 52

Figure 22 Schematic showing N_2 blanket around MOSR 54

Figure 23 Schematic showing precipitate formation upon sampling..... 57

Figure A 1 St. Michael's mine water oxidation test procedure 70

Figure A 2 Ferrous iron calibration curve..... 78

PREFACE

I would like to thank and acknowledge all the individuals who made this work possible. Dr. Neufeld for his support and facilitation of the learning process. Financial support from the Southern Alleghenies Conservancy, the PA Department of Environmental Protection Resource Recovery Consortium, and the Fraunhofer Center for Energy and the Environment. Special thanks go to the F^2 Machine Shop, Tarentum, PA, and PPC Corporation, Pittsburgh, PA, the fabricators of the bench-scale orifice spray reactor.

1.0 PROBLEM STATEMENT

Acid Mine Drainage (AMD) is a problem that has plagued surface and ground waters of many parts of the world for decades. AMD in the Commonwealth of Pennsylvania can be mainly attributed to the coal mining industry. In efforts to extract material resources from the earth, metals, such as iron, are exposed to the atmosphere. Upon atmospheric exposure these metals become insoluble resulting in precipitation. The precipitation of metals may result in many detrimental effects on the receiving body of water's quality.

As the metals precipitate they react with water. This reaction known as hydrolysis produces acidity. The acidity generated kills vegetation and wildlife. It also enhances the dissolution of surrounding strata where by more metals leach into the surface and ground waters. Upon oxidation, these metals act as an oxygen sink, depleting oxygen necessary for organisms to carry out aerobic metabolism. When the metals settle they collect on the bottom of the water body. This sludge tends to blanket the bottom of streams and drown out all benthic forms of life.

According to Pennsylvania Governor Rendell "…abandoned mines are the state's biggest source of water pollution that is killing stream and plant life, reducing the value of nearby property and making waters unusable for fishing and swimming." (Toland 2004). The projected cost for AMD remediation in Pennsylvania is between 5 and 15 billion dollars with a cleanup time of 50 years (Rossman et al., 1997).

Currently, many abandoned mine reclamation projects make use of what is called passive treatment. In general, passive treatment involves the use of wetlands or large oxidation ditches. Mine discharge is collected in a large shallow lagoon. Upon entering the lagoon, the mine

discharge is neutralized through the addition of an alkaline agent. Oxygen is provided through natural aeration from the atmosphere. Therefore the need for minimal depth, large area lagoons.

There are many problems associated with the different configurations of passive AMD treatment methods. The problems arise due to the slow reaction rates associated with passive treatment. In any ferrous containing discharge, it is recommended to precipitate the iron out of solution in the ferric form thus reducing costs associated with alkalinity addition. Precipitation of ferric iron is recommended because ferric iron is less soluble than ferrous iron at lower pH values. To convert ferrous to ferric the cheapest oxidizing agent is oxygen where it is supplied from the atmosphere. This translates to a large footprint. At many mine discharge sites the large areas of land are unavailable due to the site topography. These sites are best suited for active AMD treatment systems.

Due to the lengthy detention times required in passive treatment systems the need for an active remediation system is evident. An active system can be defined as a system, which utilizes an outside energy source to accomplish AMD treatment at a rate greater than can be found with a passive treatment method. The scope of this document is to present an efficient active treatment system for the remediation of AMD. Mechanisms for accelerated ferrous oxidation rates will be presented.

1.1 SURFACE WATER QUALITY STANDARD

Since the passage of the Surface Mining Control and Reclamation Act (SMCRA) in 1977 and the Clean Water Act (CWA) in 1972 by the United States government, operators of coal mines are required to meet environmental land reclamation standards as well as water quality standards. The SMCRA is intended for land reclamation standards while the CWA is intended for water quality standards.

Under the CWA, each mining operation must be issued a National Pollution Discharge Elimination System (NPDES) permit. Allowable contaminant discharge levels are usually determined by the U.S. Environmental Protection Agency's (EPA) technology based standards. In cases where discharges are released into surface waters with specific uses, more stringent water quality standards may be enacted by the governing regulatory agency.

NPDES permits on surface mines usually require monitoring of pH, total suspended solids, and iron and manganese concentrations. The monitoring of other constituents may be requested by the regulatory authority in a particular mining situation. The figure below shows technology based point source discharge limitations for acid mine drainage (EPA 1983).

Table 1 EPA coal mining effluent water quality

Effluent Characteristic	Maximum for Any 1 Day (mg/l)	Average of Daily Values for 30 Consecutive Days Shall Not Exceed (mg/l)
Total Iron	7	3.5
Total Manganese	4	2
Suspended Solids	70	35
pH	6 - 9	------

2.0 LITERATURE REVIEW

2.1 ACID MINE DRAINAGE CHEMISTRY

Acidic discharges were present long before coal mining operations began. The acid is formed when pyrite, iron sulfide (FeS_2), is exposed to oxygen and water. The pyrite oxidizes to form a weak solution of sulfuric acid. As this acid passes over the surrounding strata it dissolves various metals such as iron, aluminum, manganese, calcium, magnesium, sodium, and other trace metals. These metals become soluble and pollute the receiving surface water.

Another naturally occurring mineral associated with coal bearing strata is marcasite. Marcasite has an identical stoichiometirc representation as pyrite, FeS_2, but is different in crystalline structure. All though both minerals are acid producers, pyrite is much more prominent and generally associated with AMD. Pyrite is usually found naturally near coal seams.

Upon coal mining operations, iron pyrite is left exposed to water and oxygen. This exposure greatly increases the rate of natural oxidation. The consequent acidic discharge to surface waters is termed Acid Mine Drainage (AMD).

The general chemical equation describing the oxidation of FeS_2 to form ferrous sulfate and release 2 mols of sulfuric acid has been found to be:

$$FeS_2 + 7/2\ O_2 + H_2O \rightarrow Fe^{2+} + 2SO_4^{-2} + 2H^+ \qquad (1)$$

The ferrous iron eventually uses 1 mol of H+ and oxidizes to the more stable ferric form according to:

$$Fe^{+2} + ¼\ O_2 + H^+ \rightarrow Fe^{+3} + ½\ H_2O \qquad (2)$$

Above a pH of approximately 4.0, the ferric ion undergoes hydrolysis and forms a ferric hydroxide precipitate. This is represented by:

$$Fe^{+3} + 3H_2O \rightarrow Fe(OH)_3 + 3H^+ \qquad (3)$$

As a result of the processes represented by equations 1 – 3 one mol of pyrite will produce 4 mol of hydrogen ions; 2 mol from the initial oxidation of pyrite and 2 mol from the combined iron oxidation of ferrous to ferric and subsequent hydrolysis to ferric hydroxide. The 4 mol of H^+ are equivalent to 2 mol of sulphuric acid.

Figure 1 shows the solubility of ferrous and ferric iron as a function of pH. As previously mentioned it is favorable to oxidize any ferrous iron to ferric iron due to the solubility of ferric iron. The minimum solubility of ferrous iron occurs at lower pH than the minimum solubility of ferrous iron. This will lead to substantial savings in the alkaline agent requirements.

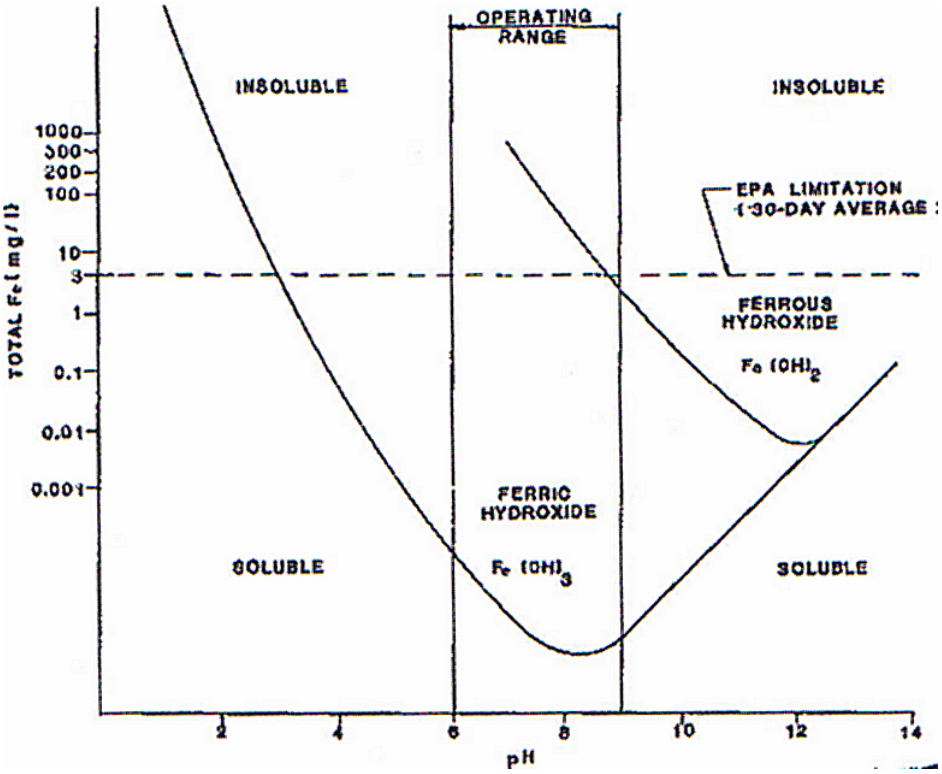

Figure 1 Ferrous and ferric iron solubility diagram

2.2 IRON OXIDATION

2.2.1 Iron Dependent Model

The kinetics of ferrous iron oxidation has previously been studied and reported to be:

$$-d[Fe(II)]/dt = k[OH^-]^2 P_{O2}[Fe(II)] \quad (4)$$

where k is the rate constant ($M^{-2}atm^{-1}min^{-1}$), $[OH^-]$ is the concentration of hydroxyl ions, and [Fe(II)] is the concentration of total ferrous iron(Stumm and Lee 1961). When pH and P_{O2} are kept constant, equation 4 can be reduced to a first order equation:

$$-d[Fe(II)]/dt = k_1[Fe(II)] \quad (5)$$

where $k_1 = k[OH^-]^2P_{O2}$ and has the units inverse time. Equation 5 can then be integrated and the following equation results:

$$[Fe(II)] = [Fe(II)]_0 exp(-k_1 t) \quad (6)$$

2.2.2 Factors Affecting Iron Oxidation

The following literature is a review of factors that affect iron oxidation and rates there of.

REACTION RATE CONSTANTS (K) As suggested by the above, any combination of engineering techniques that could increase the overall oxygen transfer coefficient (k_{O2}) and the pH dependent iron conversation rate (k), should also increase the rate of ferric iron formation.

Equation 6 shows that, when holding the pH and P_{o2} constant, the amount of ferrous iron present at any time is dependent on the value of the constant of proportionality, k_1. The k value itself depends on many factors and is empirically obtained. Therefore one must be careful in the use of experimentally obtained k values or the use of similar values from the literature.

Since the rate of ferrous iron oxidation is strongly dependent on pH, the rate constant produced can be erroneous due to pH variation within an experiment. For example, Sung and Morgan (1980) reported that initial drops in pH corresponded to the introduction of ferrous ions in solution, which is a source of strong acid protons. Later, a rise in pH is noticed due to the

diffusion of aqueous CO_2 from the solution. In treating AMD a rise in pH can be achieved due to the diffusion of aqueous CO_2 from the AMD.

IONIC STRENGTH Another factor affecting the oxidation rate is the ionic strength of the solution. A series of experiments at different ionic strengths (I) carried out by Sung and Morgan (1980) showed the variation of log k with $(I)^{1/2}$. The variation can be equated by performing a linear regression which gives:

$$\text{Log } k = 13.76 - 2.06(I)^{1/2} \qquad (7)$$

When literature values for the rate constant were used in the above equation with different ionic strengths, the equation proved to be accurate.

TEMPERATURE Temperature affects the oxidation rate as well. The rate is shown to increase as the temperature increases. When normalization of data is done with respect to changes in K_w and O_2 solubility the rate constant is shown to vary slightly with temperature (Sung and Morgan 1980).

ANIONS Anions present in solution also have an effect on the rate of ferrous iron oxidation. The rates decrease with respect to anions in the order of ClO^{4-}, Cl^-, SO_4^{2-}. Sung and Morgan (1980) showed that in a chloride media the rates increase with decreasing chloride concentrations. The fact that anions in solution retards ferrous iron oxidation rates compares positively to the work of Tamura et al. (1976) who studied the effects of anions on ferrous iron oxidation and proposed that complexation of ferrous iron by anions can account for retardation of oxygenation. Also, Liang and Kester (1961) showed that the presence of Cl^- and SO_4^{-2} anions can effectively reduce the oxygenation rate to that of seawater.

ALKALINITY The role alkalinity plays in the iron oxygenation kinetics is unclear, though it is known that it provides a buffering capacity for acidity and it contributes to ionic strength. The presence of alkalinity is important in the remediation of acid mine drainage using an active system. Alkalinity may provide a buffer which neutralizes any acidity generated upon ferrous oxidation. This buffer capacity can reduce alkaline agent requirements there by saving costs associated with AMD treatment.

OXYGEN TRANSFER As can be seen in equation 4, the mass transfer of oxygen into the liquid phase plays a strong role in the oxidation of ferrous iron and hence treatment. This section discusses the fundamentals of oxygen transfer from the gas phase to the liquid phase.

One of the most widely used theories for gas liquid mass transfer is the Lewis and Whitman two-film theory. This theory is based on a physical model in which two films exist at the gas liquid interface. The two films, one gas and one liquid, provide resistance from the passage of gas molecules between the bulk liquid and the bulk gaseous phases. It is important to note that the bulk liquid and bulk gas phases are completely mixed. A definition sketch is shown in figure 2.

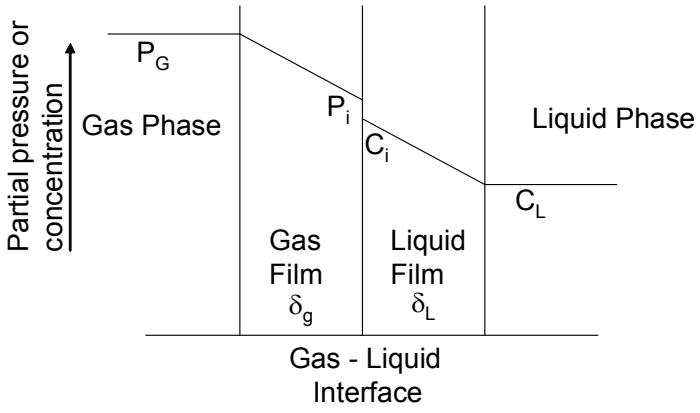

Figure 2 Two film theory of gas transfer, very slow or no chemical reaction

Under steady state, the rate of mass transfer of a gas through the gas film must be equal to the rate of mass transfer through the liquid film. From Fick's first law the mass flux for each absorption phase is as follows:

$$r = k_G(P_G - P_i) = k_L(C_i - C_L) \quad (8)$$

where r = rate of mass transferred per unit area per unit time

k_G = gas film mass transfer coefficient

P_G = partial pressure of constituent A in the bulk of the gas phase

P_i = partial pressure of constituent A at the interface in equilibrium with concentration C_i of constituent A in liquid

k_L = liquid film mass transfer coefficient

C_i = concentration of constituent A at the interface in equilibrium with P_i of constituent A in the gas phase

C_L = concentration of constituent A in the bulk liquid phase

The concentration gradients in the above equation represent the driving forces causing mass transfer in the gas phase or liquid phase. If each gradient is divided by its respective film thickness the driving force can be expressed in terms of unit thickness. Therefore if the thickness of the film is reduced the degree of mass transfer can be enhanced.

In practice it is difficult to measure the values of k_G and k_L at the interface so the overall coefficients K_G and K_L are used instead. In this work it assumed that all the resistance to mass transfer is in the liquid side so the equation becomes

$$r = K_L(C_s - C_L) \quad (9)$$

where r = rate of mass transfer per unit are per unit time

K_L = overall liquid mass transfer coefficient

C_s = concentration of constituent A at the interface in equilibrium with the

concentration in the bulk gas phase

C_L = concentration of constituent A in the bulk liquid phase

To estimate the flux of a slightly soluble gas from the gas phase to the liquid phase the above equation can be changed by swapping C_L with C_t. The new equation is

$$r = K_L(C_S - C_t) \qquad (10)$$

where r = rate of mass transfer per unit are per unit time

K_L = overall liquid mass transfer coefficient

C_s = concentration of constituent A at the interface in equilibrium with the concentration in the bulk gas phase (governed by Henry's Law)

C_t = concentration of constituent A in the bulk liquid phase at time t

The rate of mass transfer can be found by multiplying by the area and dividing by the volume, giving

$$dc/dt = K_L(A/V)(C_S - C_t) = K_{La}(C_s - C_t) \qquad (11)$$

where dc/dt = change in concentration per unit time, $ML^{-3}T^{-1}$

K_{La} = volumetric mass transfer coefficient, T^{-1}

A = area through which mass is transferred, L^2

V = volume in which constituent concentration is increasing, L^3

a = area for mass transfer per unit volume, A/V, L^{-1}

The term K_{La} depends on the liquid characteristics and type of equipment being used for mass transfer and is unique for each situation.

The above discussion for mass transfer using the film theory can be applied to the presence of no chemical reaction or a very slow chemical reaction involving an absorbed gas and a reactive chemical constituent in the bulk liquid phase. In this particular case, a slow chemical reaction,

the gaseous species is absorbed and diffuses through the film and then reacts in the bulk liquid. The process of a chemical reaction and diffusion become two steps in series when considering a slow reaction. In such a case the, absorption rate is unaffected by a chemical reaction.

Figure 3 is a depiction of the absorption process in the presence of a chemical reaction. Chemical reactions between an absorbing species and a reactant may be considered instantaneous in some cases. According to Shah (1979) the increase in absorption rate due to the chemical reaction is maximized in the presence of a chemical reaction. If the reaction between the absorbing species and the reactant is so rapid the two reagents can not coexist in the liquid then a reaction plane is formed in the liquid. The instantaneous reaction occurs and both the absorbed species and the reactant diffuse towards this reaction plane where they react.

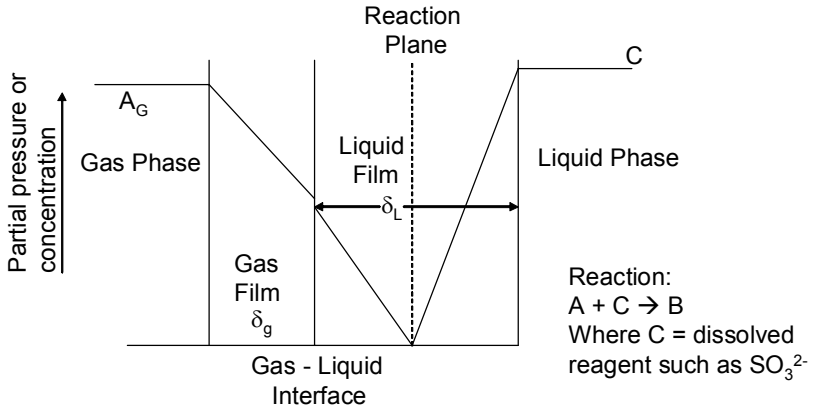

Figure 3 Two film theory, instantaneous reaction

When the concentration of reactant is much larger than that of the absorbed species the reaction plane is almost next to the gas liquid interface and the rate of reaction is governed by the rate of diffusion of the reactant from the bulk liquid to the interface.

2.2.3 Acid Mine Drainage Treatment

The purpose of this section is to present the two approaches used to treat acidic mine discharges, passive and active treatment. The treatment method used in the experiments presented in this paper is of the active type.

Figure 4 presents a typical process flow diagram for the treatment of AMD. Conventional AMD treatment consists of the following four steps: 1) neutralization, 2) oxidation, 3) settling and disposal/reuse of sludge, and 4) effluent discharge/reuse.

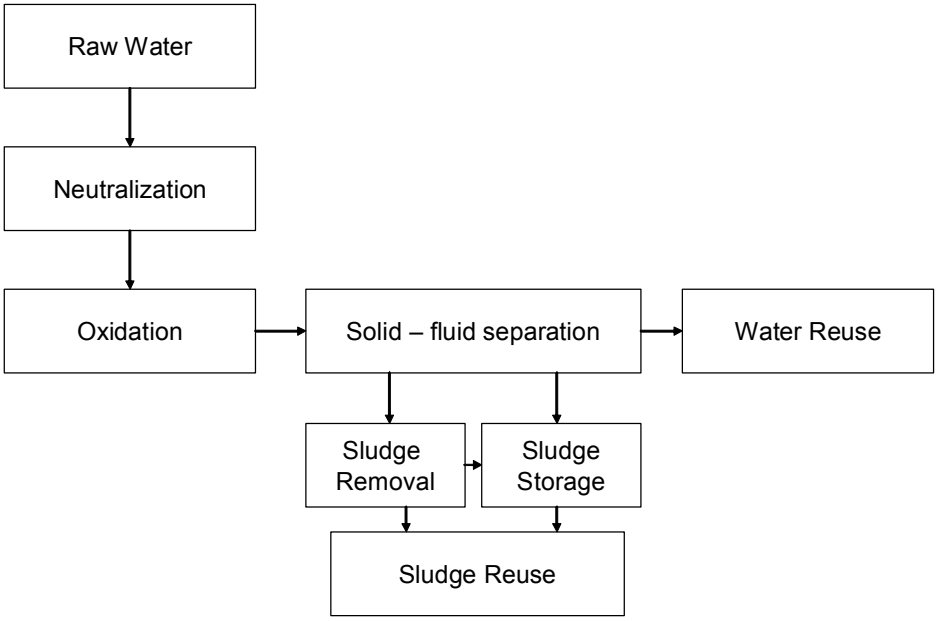

Figure 4 Process flow diagram for AMD treatment

Neutralization can be accomplished by the addition of various alkaline agents. The determining factors in selecting an alkaline agent are rate and level of pH increase desired, the solubility of the chemical in the mine water, handling, and cost. (Clarke 1995). Five of the more commonly used chemicals for neutralization are:

-calcium carbonate, $CaCO_3$ (limestone),

-calcium hydroxide, $Ca(OH)_2$ (hydrated lime),

-sodium carbonate, Na_2CO_3 (soda ash),

-sodium hydroxide, NaOH (caustic); and

-ammonia, NH_3.

Since this paper focuses on removing iron from AMD, oxidation refers to iron oxidation. As AMD is formed iron is first found in the ferrous form (Fe^{+2}). Ferric iron is much less soluble than ferrous iron and can be precipitated as a hydroxide to effluent levels below acceptable at pH values below 6.0. The minimum solubility of ferric iron occurs at a pH of 8.0. Ferrous iron does not reach minimum solubility until a pH of approximately 11.0. At a pH of 9.0, ferrous iron is soluble to about 4 mg/L. This pH value is above the maximum allowable discharge pH. Therefore, when utilizing a chemical neutralization process, it is advantageous to oxidize any ferrous to the ferric form so it can be effectively removed at a lower system pH. The methods available to accomplish oxidation are through natural or mechanical aeration, chemical oxidation, and biological systems.

The chemical equations representing the oxidation of ferrous iron to ferric and the subsequent hydrolysis are:

$$Fe^{+2} + ¼\ O_2 + H^+ \rightarrow Fe^{+3} + ½\ H_2O \qquad (12)$$

$$Fe^{+3} + 3H_2O \rightarrow Fe(OH)_3 + 3H^+ \qquad (13)$$

The stoichiometric relationship of the above two equations shows that 1 mg of oxygen will oxidize 7 mg of ferrous under ideal conditions. During this hydrolysis reaction, 1 mol of acidity

is formed for each mol of ferrous iron that is oxidized. As a result, sufficient excess alkalinity must be added during neutralization to compensate for this production of acidity.

2.2.4 Passive Treatment

Passive treatment systems are intended to treat acidic mine discharges with minimal operating and maintenance costs besides those costs procured during the initial construction. Passive AMD treatment technologies consist of the following or renditions of the following:

- Aerobic wetland,
- Anaerobic wetland,
- Open limestone channels,
- Anoxic limestone drains.

The above treatment systems rely upon abiotic or biotic processes that typically do not require metered chemical additions. In the case of abiotic oxidation in a passive system, the oxidation takes place through atmospheric diffusion of oxygen and is governed by Fick's law. Reported iron removal in passive treatment systems is between 10 – 20 $g*m^{-2}*d^{-1}$ (Heidin and Nairn 1992). This approach assumes that iron oxidation kinetics is zero order, which contradicts iron oxidation models of Stumm and Lee (1961).

2.2.5 Active Treatment

The terms "active treatment systems" have once been defined as systems that require continual addition of chemicals or continuous active water treatment (L.B. Clarke 1995). Active treatment is advantageous over passive treatment at many sites due to the smaller footprint required and the reliability of the system. Examples of two active treatment technologies are presented below. The later being the basis for the technology presented in this document.

2.2.5.1 In Line Aeration and Neutralization System (ILS)

Figure 5 shows the cross section of an active AMD treatment known as the ILS.

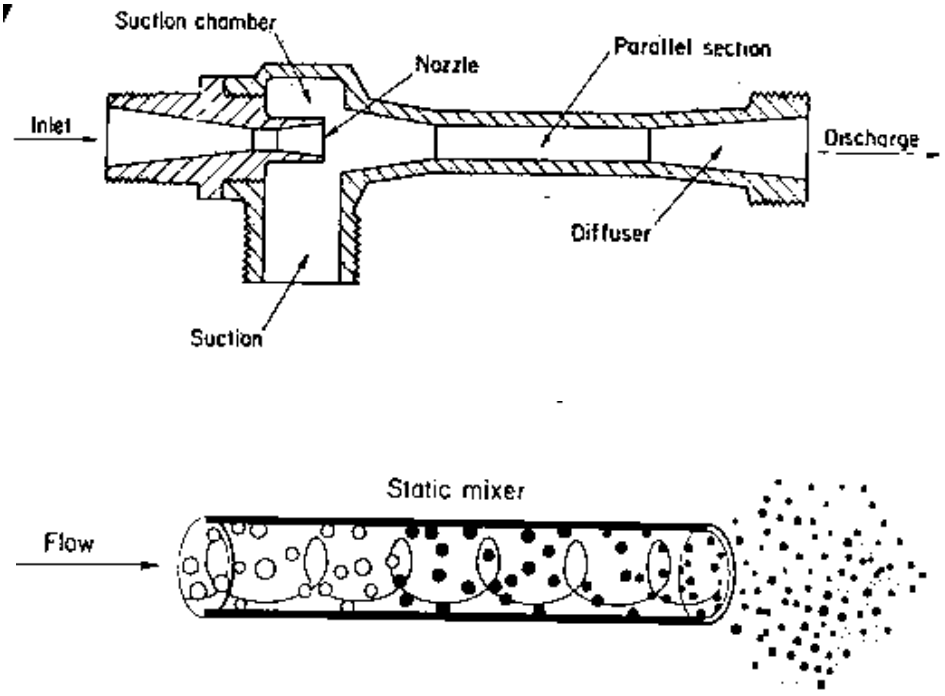

Figure 5 ILS cross section

The ILS is an in line system used to treat AMD developed by the U.S. Bureau of mines (Ackman and Kleinmann 1984). It utilizes a "jet pump" and a static mixer equipped in line. The water is aerated by air flow into the jet pump which is caused by venturi action. Water next flows through a static mixer attached to the discharge of the ILS where further aeration and mixing

takes place. An alkaline agent is injected into the suction port of the jet pump, the same place where air is inducted.

A jet pump is essentially a venturi, a nozzle with a decreasing diameter. This decreased diameter creates a back pressure (high pressure drop) which is overcome by the mine pump. The pressure is converted into a high velocity stream of water leaving the reduced diameter section of the nozzle. Due to the accelerated flow, a pressure difference occurs and as a result air is entrained into the liquid flow by venturi action. A static mixer, which is connected down stream of the jet pump, is simply a pipe with baffles placed on the inside. These baffles are arranged in a helical pattern to promote a spiraling flow of the fluid and as a result mixing occurs. The ILS was reported to work in the field as well as in the laboratory.

Hustwit et al. (1992) measured rates of ferrous iron oxidation in the ILS system. Their work shows that at concentrations below 800 mg/L the rate of ferrous iron oxidation depends on the initial ferrous iron concentration. At ferrous iron concentrations higher than 800 mg/l, the ferrous iron oxidation rate reached a maximum.

2.2.5.2 Turbojett (TJ)

Figure 6 shows the cross section of an active AMD treatment system for the remediation of AMD. This technology is what the Multiple Orifice Spray Reactor (MOSR) bench scale experiments in this paper are modeled after. The TJ is the trade name given by the inventors. The TJ is an aeration device that can be installed in line to the effluent discharge of a mine dewatering pump and is used as an active system to remediate AMD. It was patented in 1984 (US Patent Number 4474477) as a “Mixing Apparatus”.

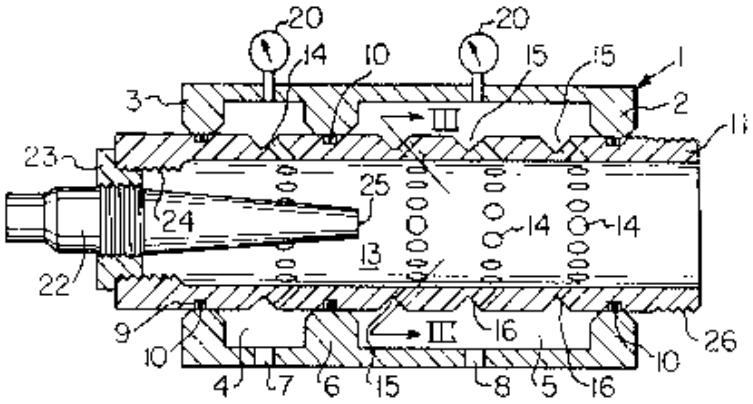

Figure 6 TJ cross section

The device consists of two concentric cylinders. In the annulus of the cylinders is where fluid (AMD water) enters the TJ into a chamber which is comprised of the two rings. The inside cylinder is hollow and is open at both ends. The inside cylinder has a number of engineered orifices arranged in such a geometry that liquid forced through these orifices is discharged having velocity components toward the exit of the cylinder, as well as a component which promotes a helical pattern. Due to the relatively small diameter of these orifices, pressure builds up on the inlet side of the TJ in a manner similar to the venturi system described above. These pressures (pressure drops) also range from approximately 30 – 100 psi, with an acceptable pressure drop of about 40psi (personal communication with the Turbojett fabricator). When the fluid discharges through the TJ it leaves as a jet spray and the pressure becomes atmospheric. It is believed that as a result of the jet moving so fast relative to the ambient air, a venturi action and water cavitation results. Also, as a result of this pressure difference, air is sucked into the center of the TJ. Inside the center cylinder where air is drawn into where the aeration and mass transfer of oxygen to the liquid phase takes place. In this fashion, the Turbojett and ILS (venturi) systems share certain operating fundamentals of mass transfer.

Also in figure 6 the chambers on the sides of the TJ where fluid enters and is then forced through the orifices can be seen (Smith and Roy 1984). The claims section of patent does not mention that this device specifically aerates water. However, the section Summary of Invention states that one application is for the addition of chemicals to wastes, such as acid mine water. It then goes on to discuss how efficient waste treatment is accomplished by the addition of chemicals to the waste and the reaction takes place in the high energy mixing area of the mixing chamber. Lastly it states that air may be used to atomize the waste materials to create small globules which will enhance the reaction of the chemicals with the substances in the waste material.

As reported in a prior International Water Conference (Pittsburgh) proceedings paper, the TJ has been demonstrated as a successful remediation technology for the treatment of AMD from the Martinka Mine located near Fairmont, West Virginia (Kolbash and Budeit 1988). This remediation effort was sponsored by American Electric Power Company. The AMD treatment system was in operation for two years and ten months. There never was a shutdown due to not meeting discharge limits. The only information presented in the article is that the NPDES discharge limits for the mine were maintained throughout the operation time which corresponded to monthly averages of 1.5 mg/L Fe and pH values between 6 and 9.

In this application, two eight inch TJ's were used. Each TJ treated 750 gpm of water at an optimum pressure of 34 psi. A hollow cone spray type nozzle was used to inject a dilute solution of sodium hydroxide into the air-suction side of the TJ. Sodium hydroxide was chosen as the alkaline agent because it does not contribute to sludge disposal problems. It is reported that each one of these TJs educts as much air as 690 cubic feet per minute. This induction of air and the forward swirling of fluid allowed the TJ to operate with no back splashing.

Treated water from the TJ was conducted to a settling basin where the pH was continuously monitored. The pH values at this location were used to govern caustic addition. A pump at the bottom of the basins was used to pump sludge back into the abandoned portion of the mine. Clarified water then flows over weirs at the far end of the settling basin and through an open channel to the polishing pond. Polishing pond water is checked for pH and turbidity before being discharged in to a local stream.

The purpose of the current research was to gain an understanding of how a system similar to the active treatment systems above works and to suggest areas of future work.

3.0 MATERIALS AND METHODS

The purpose of this section is to provide the methodology used in obtaining information on the oxidation capabilities of the MOSR. The main purpose is to differentiate between iron oxidation caused by O_2 transfer and ferrous iron oxidation that may result from cavitation caused by liquid flow through an orifice.

3.1 BENCH SCALE SYSTEM

Figure 5 shows the experimental set up of the MOSR.

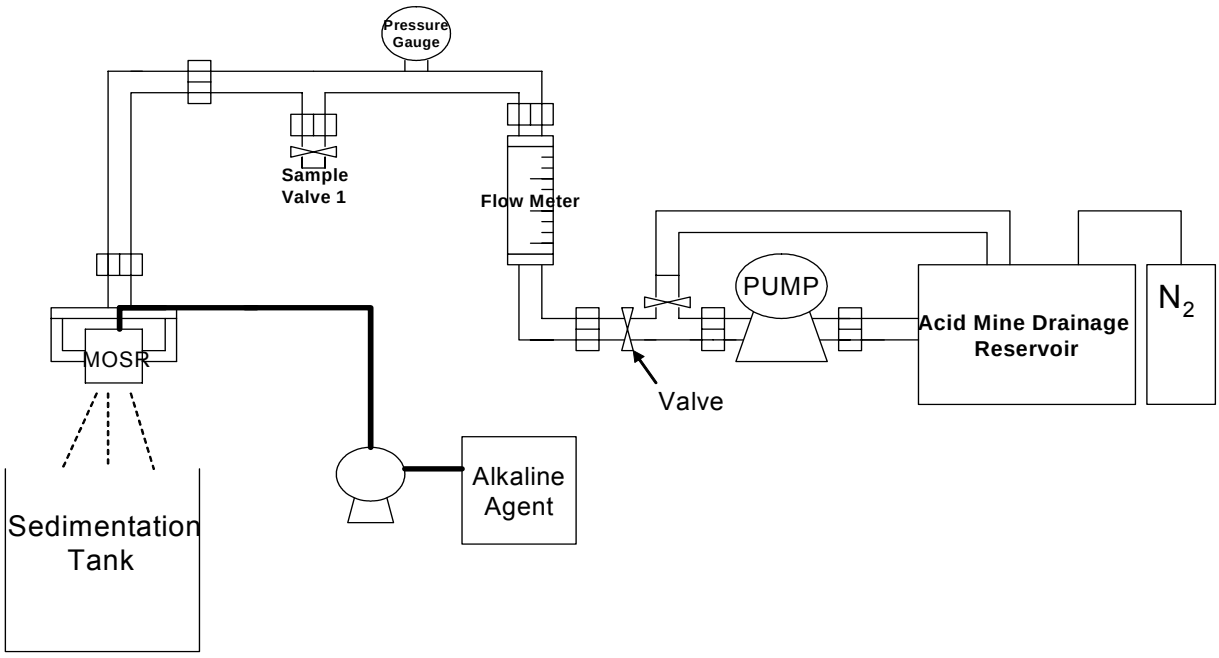

Figure 7 Experimental setup

Acid mine drainage is stored in a sealed reservoir. Nitrogen is bubbled through the reservoir to keep dissolved oxygen levels of the AMD to a minimum. Acid mine drainage is pumped from the reservoir using a SHURFLO industrial transfer diaphragm pump to the MOSR. Equipped inline are a flow meter and pressure gauge. Valves installed before the MOSR are used for in line sampling and varying the flow and consequently pressure.

Like the Turbojett the MOSR is comprised of two concentric cylinders as shown in figure 8.

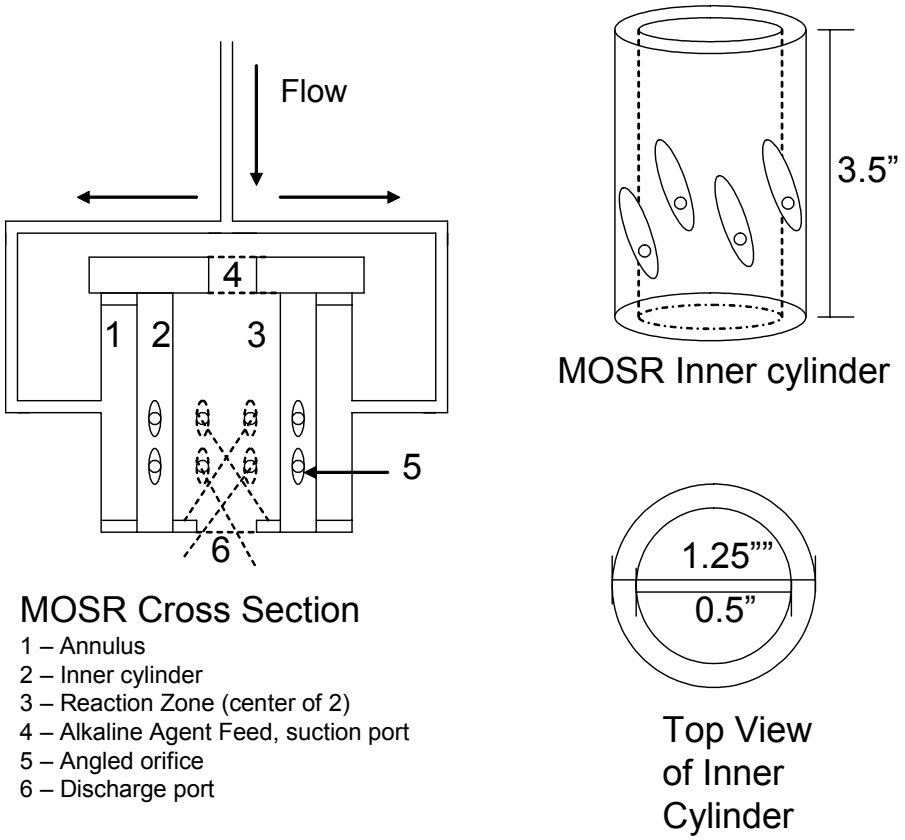

Figure 8 MOSR cross section

AMD water enters into a chamber which consists of an annulus of two cylinders (area 1, Figure 8). The inside cylinder is hollow, open at both ends, and has a number of engineered orifices (area 5, Figure 8) arranged in such a geometry that liquid forced toward the center, through the orifices, is discharged having vector components toward the discharge end of the cylinder, as well as a component which promotes a helical pattern (area 6, Figure 8).

Due to the relatively small diameter of these orifices, pressure on the inlet side of the orifices can be maintained in the range of 20 – 70 psi depending on the flow rate. The entire measured pressure drop within the experimental system is accumulated due to flow through the orifices.

To demonstrate that all the pressure generated in the system was due to the orifices, an experiment was conducted where the inner cylinder (area 2, Figure 8) was removed from the system. Water was pumped through the system at approximately 1.0 gpm with virtually no pressure drop due to bends in the piping or the geometrical configuration of the MOSR casing. The liquid discharge line is at atmospheric pressure, and leaves the reactor as a jet spray. As a result of this pressure difference a venturi action is created and air is sucked into the center of the inner cylinder where aeration and oxidation takes place (areas 3 and 4, Figure 8).

The maximum flow rate to the bench scale MOSR unit is 1 gpm (3.78 lpm). The height of the inner cylinder (reaction chamber) is 3.5 inches (8.9 cm). The annulus measured 0.25 inches (0.56 cm). The inside cylinder has two rings of orifices totaling 12 in number. These orifices are 9/16 inch (1.4 cm). The diameter of the orifices is 0.032 inch (0.08 cm) (Figure 8). Liquid enters the MOSR through two ports on the side of the MOSR as shown in Figure 8.

The residence time used in calculating the rates was based on the space time of the reactor.

Table 2 shows the calculated residence times as a function of pressure.

Table 2 Residence times of the MOSR as a function of pressure.

Pressure (PSI)	FlowRate (GPM)	Residence Time (sec.)
20	0.30	2.38
30	0.38	1.88
40	0.45	1.59
49	0.50	1.43
61	0.55	1.30
70	0.60	1.19
78	0.66	1.02

For the majority of the experiments, an aqueous solution of NaOH is introduced into the gas suction end of the MOSR through the use of a peristaltic pump. The rate of introduction of the NaOH in to the MOSR is 0.015 meq/L. This rate was determined by the stoichiometry of ferrous iron oxidation and subsequent hydrolysis of ferrous iron in which 2 mols of H^+ are produced for every mol of ferrous iron oxidized.

3.2 MINE WATER

For a series of experiments actual AMD was collected and treated in the laboratory. This water was collected from St. Michael's mine discharge. St. Michael's mine is located in Cambria County, Pennsylvania. The St. Michael's mine discharge flows into Topper Run tributary at a flow rate of 2000 – 4000 gpm (5400 – 10800 lpm). Samples (50 gallons) of AMD waters were obtained from the sampling well at the St. Michael's site and transported back to the lab in sealed containers. These samples were collected using a Guzzler diaphragm hand pump. Measurements including DO, pH, and ferrous iron were then conducted.

In order to determine the amount of alkalinity required to neutralize the samples upon treatment, a titration experiment on a 1 liter sample was carried out. This experimental procedure was suggested by the EPA (EPA 1983) to determine required residence times for treatment systems. A 1 L sample was mixed, continuously aerated, and pH was held constant at between 6.2 and 6.4 throughout the experiment. The dissolved oxygen level was maintained at between 8.9 and 9.1 mg/L throughout the experiment. Ferrous iron concentrations were measured as a function of time.

Table 3 shows the results of this experiment.

Table 3. Ferrous Iron Oxidation Test Procedure,
1 L sample of AMD continuously mixed and aerated,
pH = 6.2±0.2, DO (mg/L) = 9.0 ±0.3, T (ºC) = 19.5.

Time (min.)	$[Fe^{2+}]$ (mg/L)
0.0	124.5
1.7	56.0
5.0	21.5
7.5	14.6
13.3	5.3
16.7	4.1

This type of experiment can be thought of an oxidation and neutralization process that is employed at many abandoned mine sites. Therefore, it can serve as a comparison to the MOSR. Acid mine drainage is collected in to a holding pond and aerated. The pH is continuously monitored and adjusted using an alkaline agent as necessary.

3.3 SURROGATE AMD SOLUTION

In addition to testing mine water, which contains many unknown constituents, tests using the MOSR were conducted using synthetic mine water. This water was prepared by adding ferrous sulfate ($FeSO_4 \cdot 7H_2O$) to tap water. Ferrous sulfate was chosen due to the fact that many mine waters contain sulfate ions. The tap water was prepared in approximately 4 gallon quantities.

Prior to the addition of the ferrous sulfate deoxygenating of the tap water took place. This was done to minimize oxidation of the ferrous ions. Deoxygenating was completed using nitrogen gas. Nitrogen gas was bubbled through the enclosed container holding the tap water and was maintained throughout the experiment. The desired ferrous sulfate concentrations were added to the tap water when dissolved oxygen levels were maintained below 1.0 mg/L.

3.4 OXYGEN TRANSFER RATES

Determination of the oxygen transfer coefficient was done in a fashion similar to that of Hustwit et al. (1992). Starting with the basic relationship of oxygen transfer into water:

$$\frac{d[O_2]}{dt} = ko_2([O_2]_{sat} - [O_2]_t) \qquad (14)$$

Where k_{o2} = the oxygen transfer coefficient, sec^{-1}, $[O_2]_{sat}$ = the oxygen concentration at saturation, mg/L, $[O_2]_t$ = the oxygen concentration at time t, mg/L, and $[O_2]$ = oxygen concentration, mg/L.

A known volume of tap water was initially deoxygenated using sodium sulfite and pumped through the orifice reactor. Samples were taken immediately before entering the reactor (sample valve 1, Figure 7) and immediately after exiting the reactor. Two types of techniques for measuring oxygen transfer were employed. Oxygen transfer measurements using a DO probe and oxygen transfer measurements using SO_3^{2-}, which in the presence of an oxidant gets converted to SO_4^{2-}. Re-entrainment of O_2 was minimized by fixing a funnel directly underneath the discharge of the MOSR while holding the water level in the top of the funnel constant at the outlet of the MOSR with the water jets exiting the MOSR being submerged. This method of sampling also confined the mass transfer to the portion of spray immediately exiting the MOSR. Figure 9 is an illustration of the sampling technique employed. The use of the value of O_2 transferred, with the residence time within the chamber, resulted in a calculated oxygen transfer

rate ($d[O_2]/dt$). For calculation purposes the value of $[O_2]_t$ was taken as the average value of the DO concentration going in to the MOSR and the DO concentration immediately exiting the MOSR.

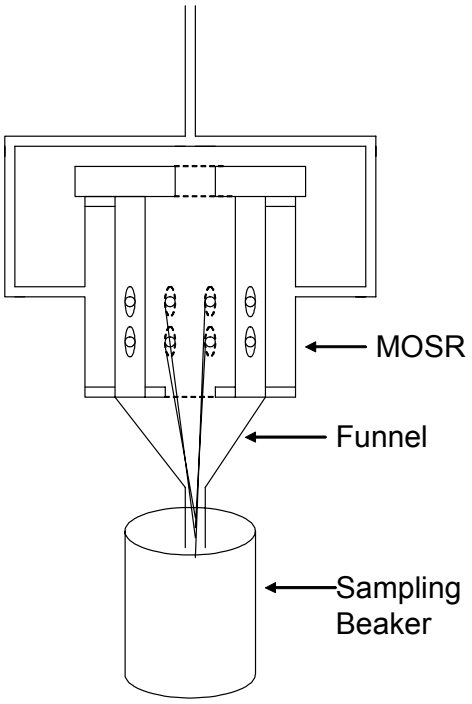

Figure 9 Schematic showing sampling

3.5 FERROUS IRON OXIDATON RATES

Ferrous oxidation rates using the MOSR were measured experimentally. The ferrous oxidation rate using the MOSR was compared to the predicted rate using a rate constant k = 3.0E-12 $minute^{-1}mol^{-1}$ (Hustwit et al. 1992) at 20 ˚C. The experimental ferrous iron oxidation rates are computed by measuring the change in ferrous iron concentrations between the influent and

effluent of the MOSR. This change in ferrous iron concentration is then divided by the hydraulic residence time to determine ferrous oxidation rates.

Aqueous samples were taken and analyzed for ferrous iron concentrations at the following points: prior to entering the MOSR (sample valve 1, figure 7) and upon leaving the MOSR. Ferrous iron determinations were conducted according to Standard Method's procedure #3500-"Fe B-Phenanthroline" (APHA et al 1998). Sampling containers were prepared with 2 mL concentrated HCL per mL of sample to limit further ferrous iron oxidation prior to analysis.

4.0 RESULTS AND DISCUSSION

This section describes the results of the experiments that were conducted using the MOSR. The experiments were conducted to show that the results of ferrous iron oxidation are greater than can be explained by the O_2 transfer capabilities of the system.

4.1 MOSR HYDRAULIC CHARACTERISTICS

Figure 10 shows the flow rate as a function of pressure for the experimental MOSR setup. The flow rate, in gpm, is plotted on the ordinate and the pressure is on the abscissa. The pressure was controlled through the use of a restricting valve and the maximum operating pressure was 75 ± 5 psi and a minimum operating pressure at 10 psi. Maximum pressure experienced in the system is due to the physical limitations of the pump used which is rated at 1.1 gpm at 0 psi.

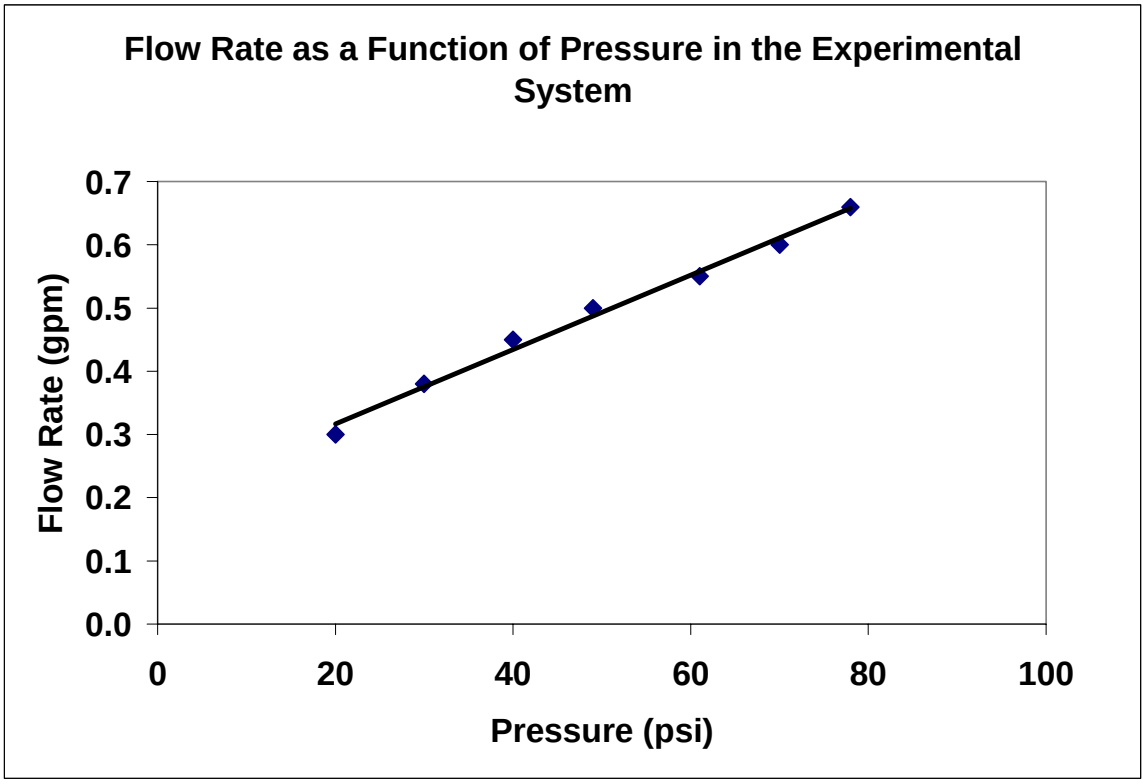

Figure 10 Flow rate as a function of pressure. The max. pressure is 75 psi due to the physical limitations of the pump used (1gpm = 3.785 Lpm).

Figure 11 shows images of the inner cylinder of the MOSR at different operating pressures. These images were taken with a digital camera retrofitted with a 10x microscope lens. From these pictures, it can be seen that the flow through each orifice is not uniform. These non-uniformities may be a result of the inconsistencies encountered upon fabrication of the MOSR unit. One of the challenges faced was drilling such small diameter holes with out cracking the inner cylinder (personal communication with MOSR fabricator, Frank Calizzi).

As the upstream pressure increases, the individual flow images change slightly. The width of the sprays changes, increasing with an increase in pressure. Another notable feature with in the

sprays is the presence of dark streaks with in the sprays. The prominence of these dark streaks increases with an increase in pressure. These streaks may be a result of the spray becoming thicker as the volumetric liquid flow rate increases.

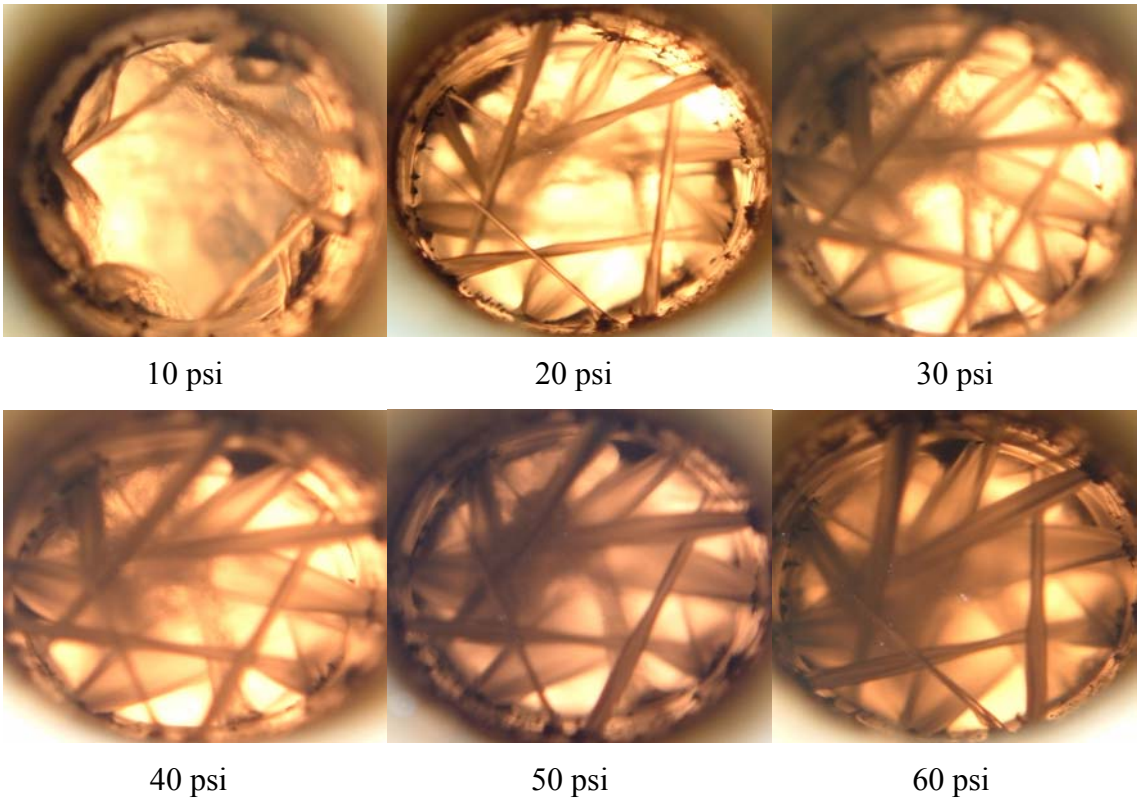

Figure 11 Images of the inner cylinder of the MOSR at various pressures.

The flows that result from liquid flow through the orifice meet in the inner cylinder, collide, mix, and in a turbulent manner produce a spray which exits the MOSR. This mixing action is an important feature of the MOSR as it provides for adequate mixing and neutralization when NaOH is injected into the reaction zone.

Figure 12 shows the views of sprays exiting the experimental MOSR at different operating pressures. As the pressure increases the sprays become more of a jet like spray. These pictures provide evidence of an increased surface area due to the formation of liquid jets having a unique droplet size distribution. The increased interfacial surface area resulting from a droplet size distribution leads to greater rates of mass transfer for field application.

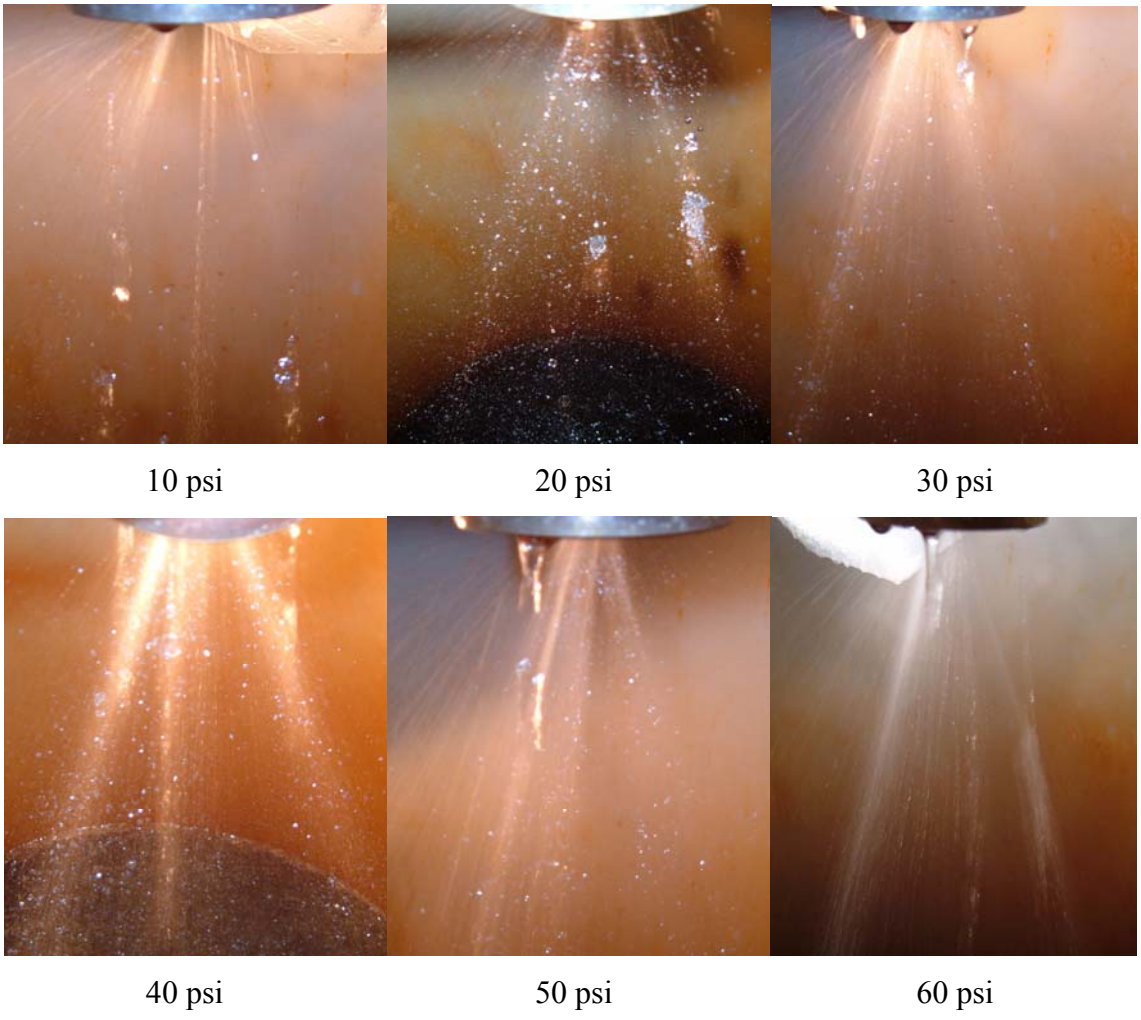

Figure 12 Exit sprays of the MOSR at different pressures.

One thing that can be noted from the images in figures 11 and 12 is that the increased benefit in mass transfer due to a change in droplet distributions or spray patterns as pressure increases is substantial from 20 psi to 70 psi but marginal as the pressure changes by 10 psi. This fact should be considered when defining an operating range for the field application of the MOSR.

4.2 OXYGEN TRANSFER CAPABILITIES

Three types of oxygen transfer experiments were carried out. Oxygen transfer in the spray immediately exiting the MOSR, with and with out a chemical reaction, and in the bulk liquid. The latter is the common approach for measuring K_{La} for aeration equipment.

Figure 11 shows the results of experiments that were carried out to measure the oxygen transfer as the spray immediately exits the MOSR at different operating pressures. From the oxygen transfer measurements k_{La} values are computed. The measurements in these experiments were carried out using a DO probe. This procedure mimics oxygen transfer in the presence of no chemical reaction, which can be modeled by the Lewis and Whitman model in the literature review.

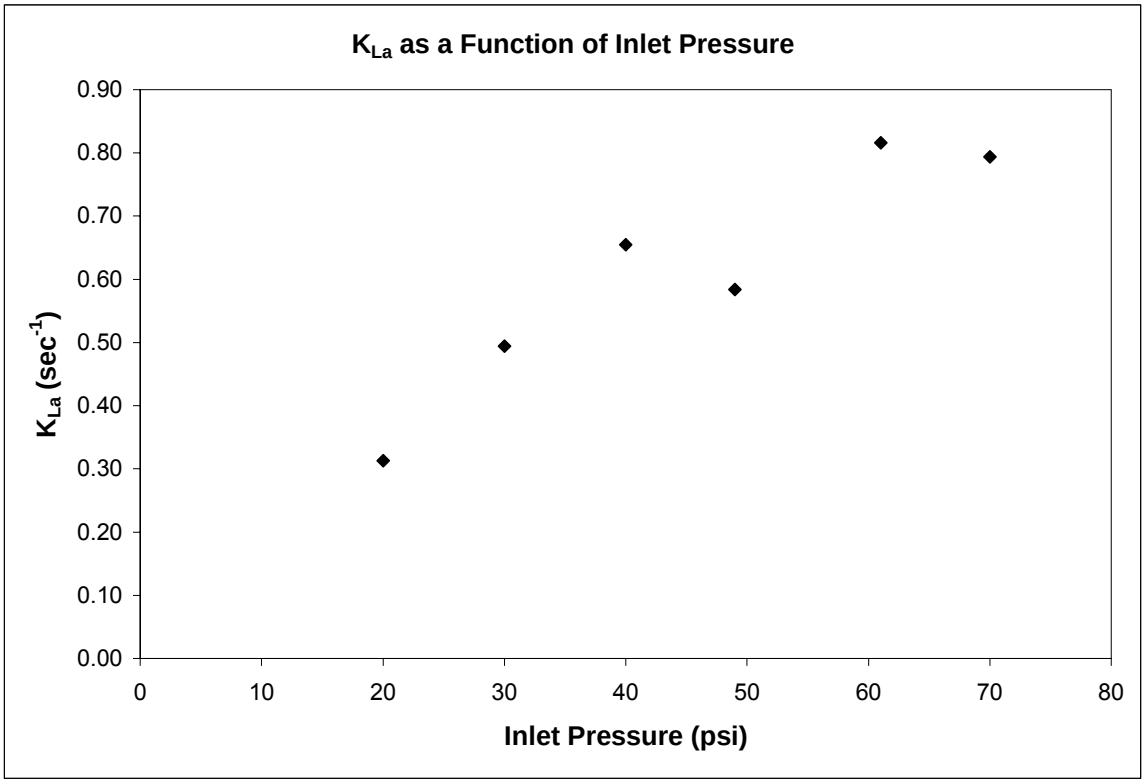

Figure 13 Oxygen transfer measurements of the MOSR at different operating pressures. T(°C) = 23.5, $[O_2]_{sat}$=8.7 mg/L.

From figure 13 it can be seen that the k_{La} values for the MOSR increase as a function of pressure until they remain constant after 60 psi. At 50 psi, the data point does not seem to follow the trend of the other points. The reason the data point does not follow the trend is because the way in which $[O_2]_t$ was measured as mentioned in section 3.4. It is the average of the DO concentration going in to the MOSR and the DO concentration coming directly out of the MOSR. The initial DO values going into the MOSR were lower in the measurements corresponding to 50 psi due to a greater amount of de-oxygenation. As a result, the $[O_2]_t$ is smaller making k_{La} smaller.

An identical experiment, at 70 psi, was conducted using no Na_2SO_3. Nitrogen gas was used to de-oxygenate the water and was continued through out the experiment to prevent any O_2 transfer. The water was then pumped through the MOSR and the O_2 transferred was measured. The results gave a K_{La} value of 0.91 $sec.^{-1}$ at 28 $^{\circ}C$. These results are comparable to the experiment, at 70 psi, using Na_2SO_3 as the deoxygenating agent.

In order to demonstrate that all the mass transfer was taking place in the reaction zone of the MOSR, an experiment was conducted where the suction port was sealed with a stopper preventing inlet air flow. The water was deoxygenated as previously described and any changes in oxygen were measured across the MOSR. The measured oxygen transfer across the system was around 0.9 mg/L D.O. This relatively small quantity of oxygen transfer may be from oxygen transfer occurring due to laboratory manipulation of the samples. However the results indicate that the bulk of mass transfer of oxygen takes place in the reaction zone.

A similar test was conducted to measure the immediate oxygen transfer of the MOSR system in the presence of a chemical reaction. This test measured the change in SO_4 before and after the MOSR and this value was used to determine an equivalent amount of O_2 transferred based on the stoichiometric conversion of SO_3^{2-} to SO_4^{2-} in the presence of oxygen. The stoichiometric equation referred to is:

$$SO_3^{2-} + 1/2O_2 \rightarrow SO_4^{2-} \qquad (19)$$

Sodium sulfite and a pinch of cobalt chloride were added to the water. When the DO read 0.5 the test was begun.

Three-hundred mL BOD bottles were used as sampling containers. After sample collection these bottles were sealed and capped until analysis. To each sample bottle 5 mL 37% HCHO was added. The formaldehyde was added to stabilize the sulfite containing solutions so measurements could be conducted.

The samples collected at the outlet were collected by fixing a funnel underneath the MOSR and filling the BOD bottles from the funnel. After the samples were collected the bottles were capped. 1 mL sample was taken from the bottles and diluted 10 times and the HACH SO_4 reagents were added to the 10 mL.

The final pH values of the samples were above 11.5. This high pH signifies that all the SO_3 has been depleted. HCHO reacts with Na_2SO_3 as follows:

$$HCHO(aq) + Na_2SO_3 + H_2O \rightarrow Na(O_3SOHCH_2) + NaOH \quad (15)$$

$$NaOH + NaHSO_3 \rightarrow Na_2SO_3 + H_2O \quad (16)$$

The NaOH is produced almost immediately in reaction 20. In reaction 21, more Na_2SO_3 is produced. This product reacts again with HCHO until there is no more SO_3 production. At this time there will be excess NaOH and the pH will be relatively high.

The results of the sulfite oxidation experiment are shown in table 4.

Table 4 Results of sulfite oxidation in the MOSR. P (psi) = 72, $[O_2]_t$ = 0mg/L.

Sample	Temperature (ºC)	Initial SO_4 Concentration (mg/L)	Final SO_4 Concentration (mg/L)	Change in SO_4 (mg/L)	Equivalent Amount of O_2 Transferred (mg/L-sec)	k_{La} (sec^{-1})
1	22	237	561	324	55	6.3
2	22	246	578	333	57	6.5
3	22	246	578	333	57	6.5
4	22	237	317	80	14	1.6
5	22	237	465	228	39	4.5
6	22	246	387	141	24	2.8
Average		241	481	240	41	4.7
Std.Dev.		5	111	109	19	2.1

Samples 1 -3 and 4 – 6 represent two different experiments. The fact that in both experiments the initial SO_4^{2-} concentrations were around the same value may suggest that the experimental procedure was valid. Between the final SO_4^{2-} concentrations for the two experiments there is large variability between the data. Despite this, the k_{La} value at 70 psi is between 6 – 9 times (k_{La} at 70 psi using SO_3^{2-} ± standard deviation / k_{La} at 70 psi using DO probe) larger than the k_{La} value at 70 psi when the measurement is conducted using a DO probe, i.e. no chemical reaction is taking place.

The larger oxygen transfer value obtained when the measurement was done by measuring the conversion of SO_4^{2-} may be due to the fact that a fast chemical reaction is taking place within the liquid. Oxygen around the liquid containing SO_3^{2-} reacts with the SO_3^{2-} almost instantaneously. The fact that there is excess SO_3^{2-} in the liquid means the O_2 concentration at any time when there is excess SO_3^{2-} will be zero. This will maximize the O_2 concentration gradient and maximize the rate of oxygen transfer.

In the presence of an instantaneous reaction involving O_2 within a liquid element a very important effect has to be considered, the mass transfer of O_2 into the liquid phase may be enhanced. If there is an excess amount of a reagent which reacts with oxygen, then the O_2 concentration gradient is maximized and hence O_2 transfer is maximized. Absorption in the presence of a slow reaction or no reaction takes place when the absorbed species diffuses completely into the liquid film before a reaction can consume its concentration. This could be thought of as what takes place when oxygen transfer is measured using a DO probe. In this case the rate of O_2 transfer may not be at a maximum.

Another explanation for higher rates of oxygen transfer when using SO_4^{2-} to measure oxygen transfer may be due to the fact that oxidation is taking place in a vapor phase. As the liquid flows through the orifices the velocity of the liquid increases. This increased velocity results in an associated pressure drop. If the local pressure falls below the vapor pressure of water then cavitation may occur. In the occurrence of this vapor zone increased oxidation may result as a result of a gas phase reaction.

Information regarding the overall K_{La} value was also obtained. For this experiment a water volume of 4 gallons was deoxygenated and recycled through the system. Dissolved oxygen measurements were measured in the bulk liquid. The overall K_{La} incorporates mass transfer from the spray and mass transfer occurring at the interface between the bulk liquid and the atmosphere. The surface mass transfer is affected by the turbulence at the liquid surface due to the jet sprays. This idea is depicted pictorially in figure 14.

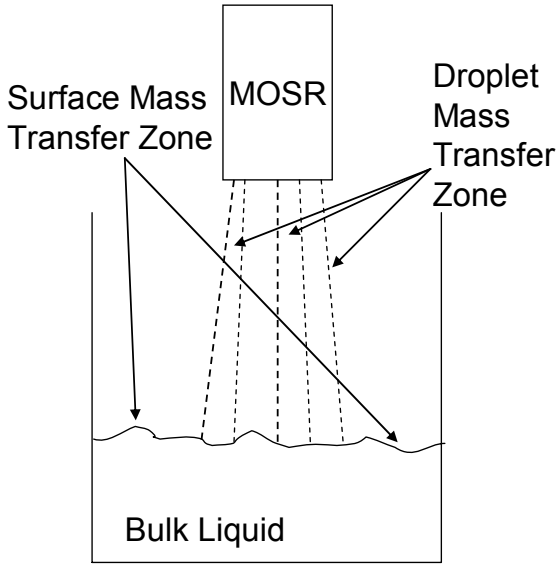

Figure 14 Mass transfer zones in the MOSR

This experiment was conducted to show there is a difference between mass transfer in the sprays and in the bulk liquid, as expected. Mass transfer at the surface takes place due to turbulence from the jets interacting with the surface. For measurements of the overall K_{La} the method using the DO probe was used. The reported value of K_{La} overall was $0.0007 sec^{-1}$.

In the case of a fast or instantaneous chemical reaction the absorption of O_2 and subsequent chemical reaction takes place during droplet flight. If an excess amount of reagents are present, after flight probably every liquid element does not contain any dissolved O_2. Any subsequent oxidation taking place in the bulk liquid would be due to the diffusion of oxygen through the bulk liquid surface, as governed by Fick's Law.

4.3 FERROUS IRON OXIDATION

A series of experiments were conducted using synthetic mine water and St. Michael's mine water to evaluate the ferrous iron oxidation kinetics in the MOSR.

4.3.1 Hydrolysis

One factor affecting the treatment process of the MOSR is the acidity generated upon precipitation of iron from solution. As seen in the stoichiometry, both Fe^{+2} and Fe^{+3} generate acidity upon hydrolysis:

$$Fe^{+2} + 2H_2O \rightarrow Fe(OH)_2 + 2H^+ \quad (17)$$

$$Fe^{+3} + 3H_2O \rightarrow Fe(OH)_3 + 3H^+ \quad (18)$$

Upon oxidation of Fe^{+2} to Fe^{+3} by oxidizing agents such as O_2 (eq. 2) or H_2O_2 one mol of acidity is consumed. Therefore it is important to fully oxidize all reduced iron in the treatment process in order to reduce acidity generation.

Table 5 shows the results of a hot peroxide titration to pH = 8.4, a method for determining acidity in a water sample (APHA et al. 1998).

Table 5 Results of hot peroxide titration on St. Michael's mine water sample.

Fe^{+2} Concentration (mg/L)	Theoretical H^+ Production (eq/L)	Hot Titration to pH = 8.4, Experimental H^+ Production (eq/L)	Percent Difference
138	0.0049	0.0055	10.5

The results show that the acidity of the sample at an iron concentration of 138 mg Fe^{+2}/L is 0.0055 eq/L. Using the stoichiometric relationship for alkalinity required (2 mols H^+ produced for every mol of Fe^{+2} oxidized) the theoretical amount of alkalinity required is 0.0049 eq/L. Approximately a 10% difference is noticed between the measured and theoretical values. The discrepancy in results may be due to the fact that there is a small amount ferric iron in the sample which contributes to acidity.

In most of the experiments conducted the amount of alkalinity used in the MOSR was held constant at a rate of 0.015 eq/L. An AMD flow rate of 0.7 gpm (the MOSR flow rate associated with maximum operating pressure) and a concentration of 138 mg/L, assuming all the iron is precipitated as ferrous, correspond to an alkalinity dose of 0.015 eq/L. Under these conditions the alkalinity dose used in conjunction with the MOSR is in agreement with the theory. In most of the experiments the caustic concentration and flow rate were kept constant even though the AMD parameters changed and hence the theoretical alkalinity demand. This resulted in a variable effluent pH. In practice the effluent pH of AMD should be in the range of 6 – 8.

4.3.2 Mine Water

A set of experiments were conducted to measure the actual MOSR's ferrous iron oxidation rates as a function of pH. This was accomplished by the introduction of calibrated levels of sodium hydroxide into the suction side of the MOSR. Six experimental trials were conducted with varying normality of sodium hydroxide in each trial. The pH (figure 15) is the final pH measured at the immediate outlet of the MOSR. As before samples were collected in acid containing vessels to prevent further ferrous iron oxidation thus isolating the influence of the MOSR for iron conversion considerations.

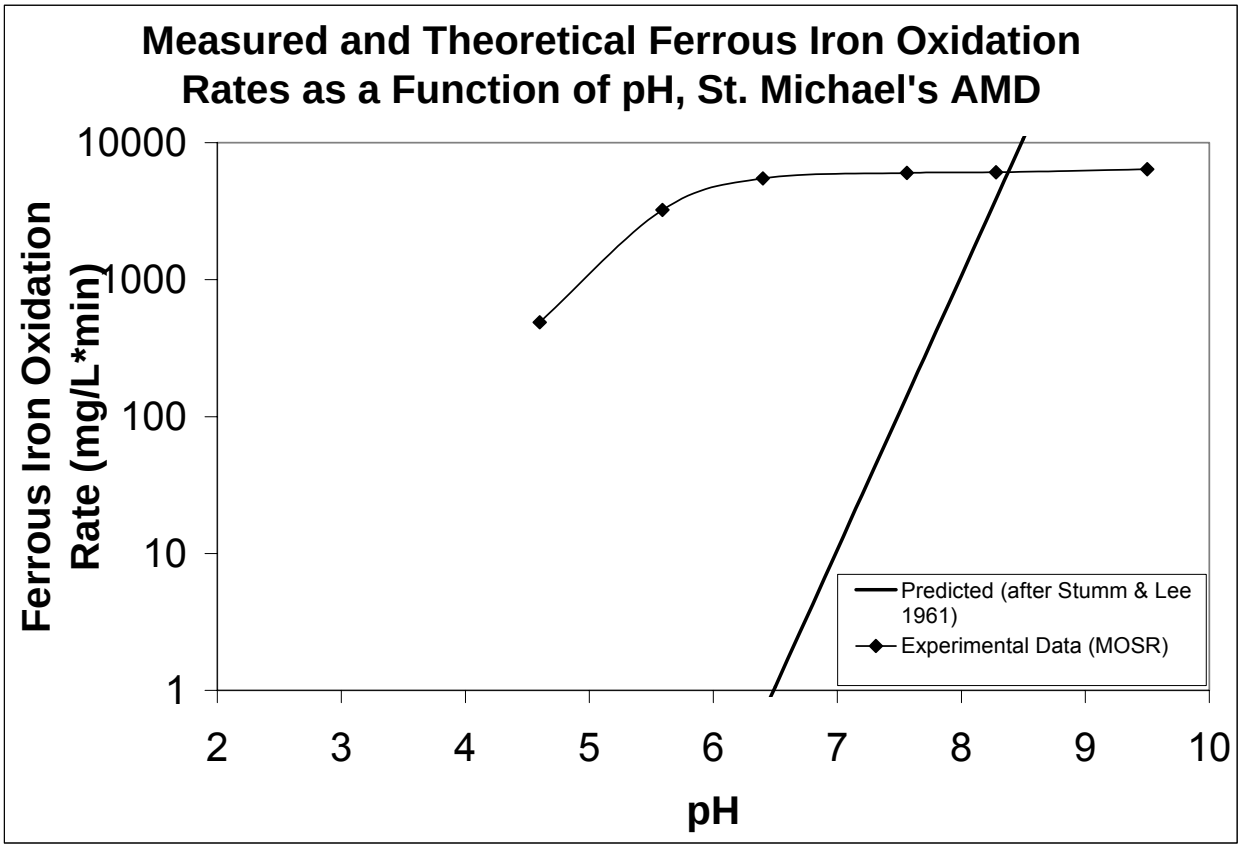

Figure 15 Ferrous iron oxidation rates, theoretical and experimental. T(°C) = 22 °C, P(psi) = 70 ± 5

Data from the Stumm model (Stumm and Lee 1961) compared to results from the MOSR, suggest that the ferrous oxidation rate is about 3.5 or more orders of magnitude greater than predicted at pH of 6.5 or less. This kinetic advantage diminishes as the pH approaches 8.0.

The mechanism for elevated reaction rates is suggested by the observation of some $Fe(OH)_2$ in the MOSR effluent. Sodium hydroxide is injected directly into the throat of the MOSR resulting in localized and temporal elevated pH values. It is likely that the Fe^{+2} precipitates as $Fe(OH)_2$ in this zone. One explanation of the increased oxidation rates in Figure 15 may be due to the presence of $Fe(OH)_2$. It is well known that hydroxo complexes of metal ions are oxidized faster by O_2 than simple aqueous metal ions (Stumm and Morgan 1996) which may explain why ferrous hydroxide is rapidly converted to ferric ion with in the 1 second detention time with in the MOSR. A similar phenomenon was likely present in the ILS reported by Ackman and Kleinmann (1984), who state that as the NaOH is injected into the ILS the instantaneous pH was extremely high. In that case, as with this research, $Fe(OH)_2$ was formed followed by ferrous to ferric iron conversion.

A second reason for the increased oxidation rates may be due liquid flow through an orifice. As water flows through an orifice increased surface areas result. Even though the method of sampling used (collecting samples immediately exiting the MOSR) minimized the effect that the jet sprays (surface area) has on mass transfer, not all of the effects could be eliminated. For example, when the MOSR is operating and sampling at the MOSR exit is being conducted fine sprays and mists exist between the orifices and the sampling container. It is assumed that these sprays have a larger surface.

Also as previously mentioned in section 4.2, there may be a vapor phase that exists near the orifices as a result of cavitation. If a vapor phase does exist it would enhance the rate of ferrous iron oxidation due to greater rates of oxygen diffusion in the vapor phase than in the liquid phase.

4.3.3 Oxidation as a Function of Pressure

In order to account for the difference in the resulting [OH^-] differences due to a varying AMD flow rate the NaOH concentration was adjusted accordingly based on the flow rate of AMD. The NaOH flow rate was not adjusted due to the physical limitations of the alkaline agent pump, a minute change in the position of the dial controlling pump speed resulted in a large change in flow rate. The change in ferrous iron and associated oxidation rates as a function of pressure can be seen in Figure 16.

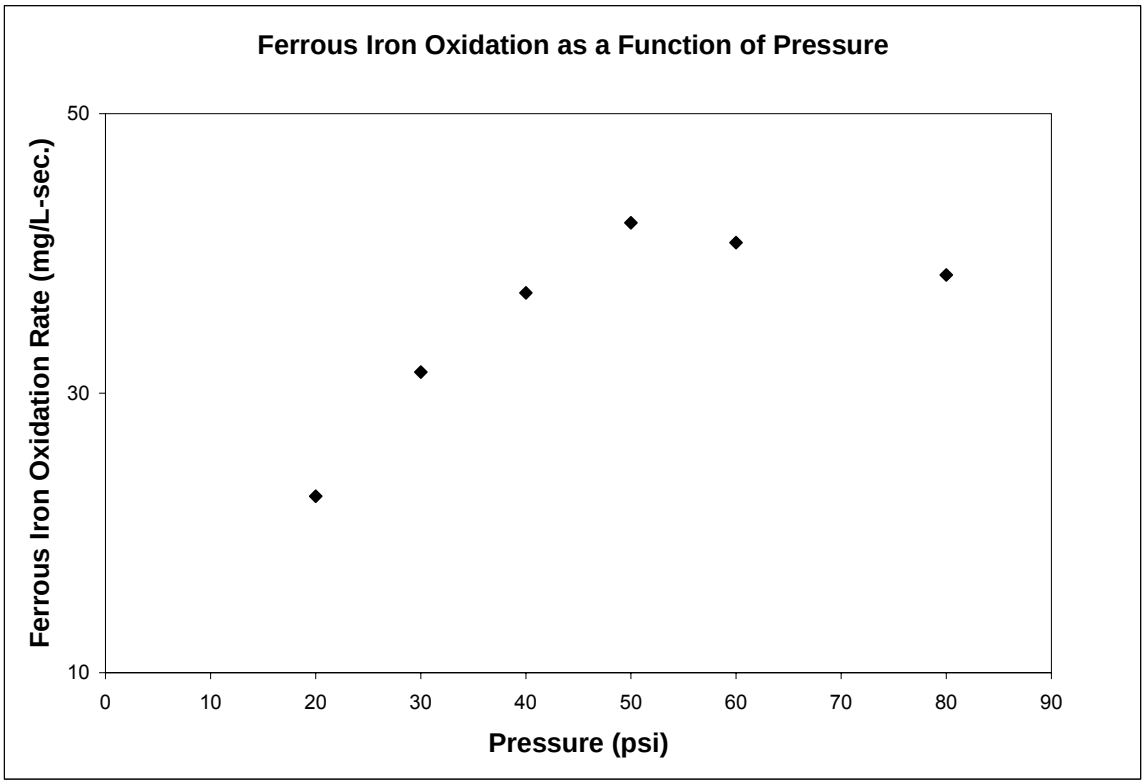

Figure 16 Ferrous iron oxidation as a function of pressure. [Fe^{+2}] = 150 mg/L, pH = 8.8±0.5, NaOH flow rate = 150 mL/min.

From Figure 16 it is seen that after 20 psi there is no substantial change in ferrous iron oxidation. When the amount of ferrous iron oxidized is adjusted to the corresponding residence time associated with each pressure the rate of oxidation increases and seems to level off after 50 psi.

Figure 17 shows the change in K_{La} and change in iron oxidation rate as a function of pressure. The changes in oxygen transfer and changes in iron as a function of pressure follow the same trend. This suggests that oxidation with in the MOSR is most likely due to oxygen transfer which is enhanced due to flow through an orifice. The k_{La} data point at 50 psi is lower due to the explanation given in section 4.2.

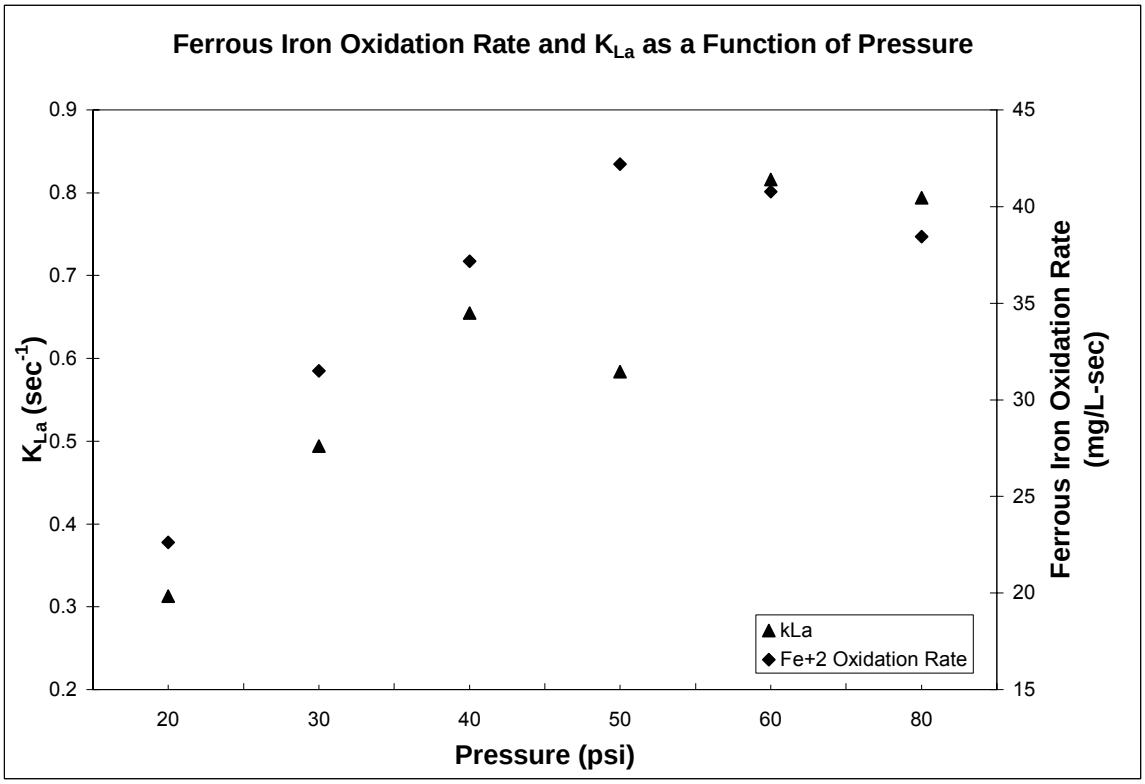

Figure 17 Oxygen Transfer and iron oxidation as a function of pressure. K_La measured using a DO probe. $[Fe^{+2}]$ = 150 mg/L, pH = 8.8±0.5, NaOH flow rate = 150 mL/min.

Figure 17 suggests that the MOSR can be operated at a pressure as low as 50 psi and still achieve oxidation rates comparable to an operating pressure of 70 psi. A lower operating pressure will result in substantial economic savings in pumping costs.

4.3.4 Oxidation as a Function of Time in MOSR Effluent

This section reports the ferrous iron oxidation kinetics of the MOSR effluent as a function of time. An experiment was conducted where a 1 L sample of MOSR effluent was collected immediately after exiting the MOSR. After collection the sample was continuously mixed and the pH, DO, and ferrous iron concentrations were measured as a function of time. For comparison a control sample consisting of a 1 L beaker of AMD was prepared at an initial concentration of ferrous iron approximately equaling the initial ferrous concentration used in the MOSR experiment. The control sample was mixed, aerated, and the pH was held constant. Figure 18 shows the results of the experiments with the MOSR and the control sample.

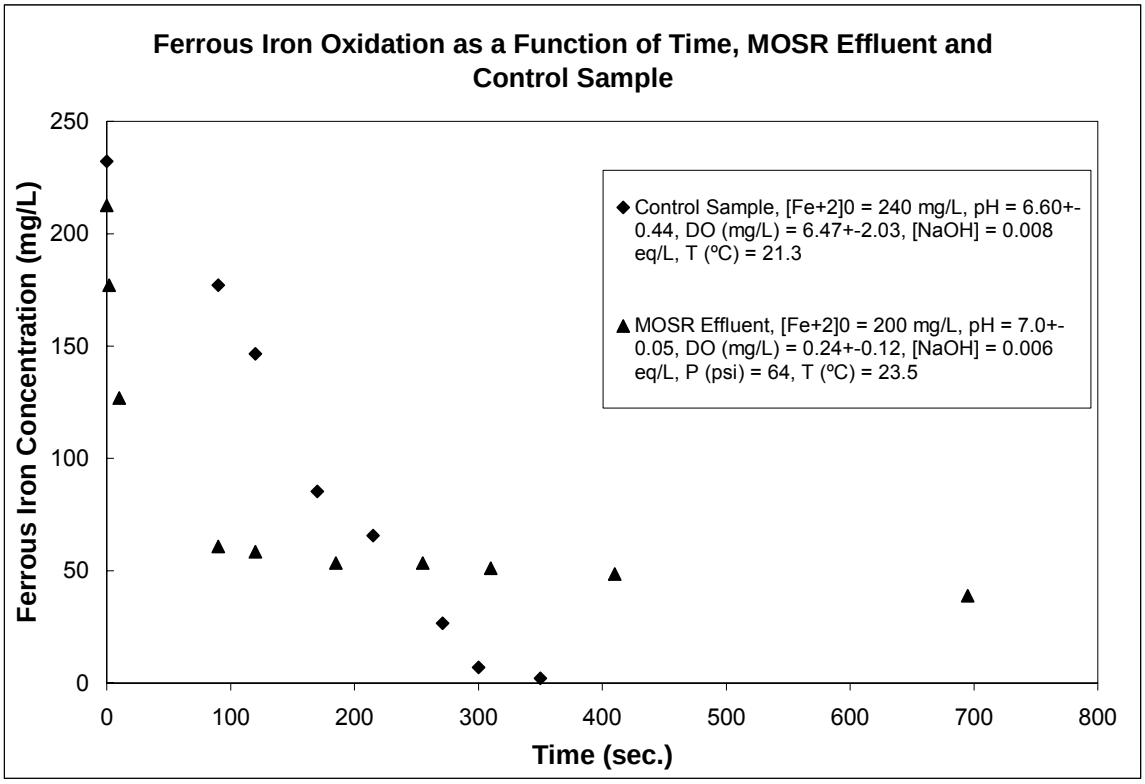

Figure 18 Ferrous iron oxidation as a function of time, MOSR effluent and an aerated control sample

Figure 18 shows the increased oxidation rates accomplished by using the MOSR. The first three points of the MOSR data represent the initial ferrous iron concentration, the ferrous iron concentration immediately exiting the MOSR, and the ferrous iron concentration in the MOSR spray just before reaching the water surface in the sedimentation tank, respectively. These three points represent the fact that the increased ferrous iron oxidation due to the MOSR takes place as the liquid elements, with increased surface area due to flow through an orifice, emanating from the MOSR traverse through an infinite volume of oxygen. Once the drops come together in the sedimentation tank the surface area is greatly increased and the ferrous oxidation is limited most likely due to decreased rates of mass transfer and hence limited oxygen supply. This can be seen at time equal to 100 seconds in Figure 18. The data at and after t = 100 seconds represents the oxidation taking place in the sedimentation tank. As can be seen in Figure 18 the rate of

oxidation is much greater than the control. The control sample can be thought of as a conventional AMD treatment technology where the pH is maintained constant and the DO levels are maintained above zero. One reason for the ferrous iron concentration reaching zero in the control sample is the control sample received approximately 0.008 meq/L caustic where as the MOSR effluent received approximately 0.006 eq/L caustic. Over the length of the experiment the pH of the MOSR effluent remained at a circumneutral pH value.

Figure 19 represents the dissolved oxygen and pH values in the MOSR effluent sample as a function of time. As time elapses the pH values in the bulk liquid decrease to a certain point. This decrease in pH may be associated with continual ferrous iron oxidation taking place in the bulk liquid. During this time the dissolved oxygen remains at zero as the oxidation continues until the point where the ferrous iron oxidation reaction no longer continues due to an unfavorable pH value or all the ferrous iron in the bulk liquid has been converted to ferric. At this point the dissolved oxygen in the bulk liquid increases, as can be seen in Figure 19.

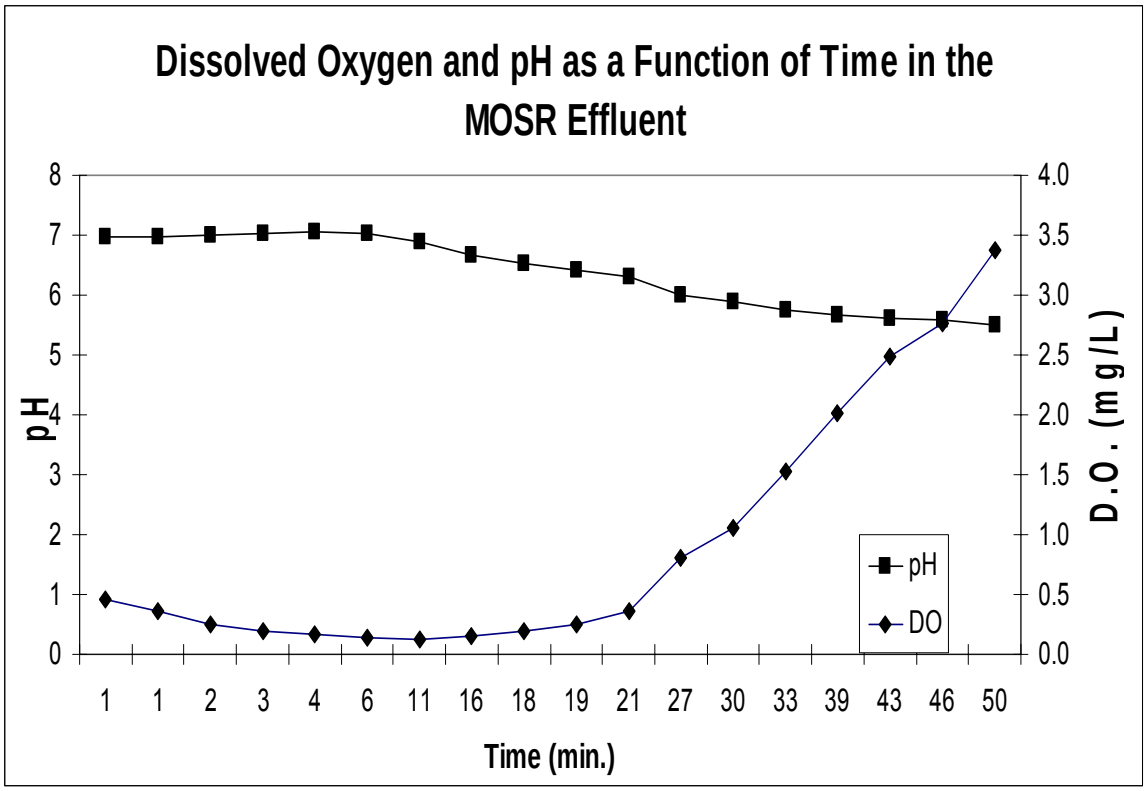

Figure 19 Dissolved oxygen and pH values as a function of time in the MOSR effluent bulk liquid

There are three zones in the MOSR where oxidation takes place. These three zones are the primary oxidation zone, immediately in the MOSR, the secondary oxidation zone in the spray exiting the MOSR and before entering the bulk liquid, and the tertiary oxidation zone in the bulk liquid of the sedimentation tank. These three zones are shown in Figure 20.

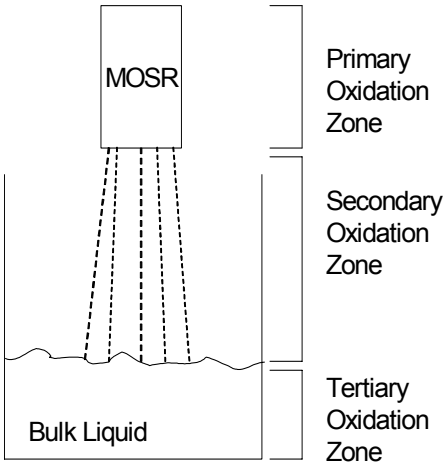

Figure 20 Zones of oxidation in the MOSR

As shown earlier, approximately 30% of the ferrous iron oxidation takes place in the primary oxidation zone. This primary oxidation is most likely the result of cavitation. The remaining oxidation takes place in the spray exiting the MOSR.

4.3.5 The Effect of Ferrous Concentration on Oxidation

An experiment was carried out to test the effect of initial ferrous iron concentrations on the effect of oxidation as ferrous iron solution flows through the MOSR. The purpose of this experiment was to quantify the maximum change in ferrous iron produced from the MOSR. Different initial ferrous iron concentrations were tested ranging from 50 – 1500 mg/L. The NaOH concentration (0.1 M) and flow rate (150 mL/min) were kept constant throughout the experiments. The pressure of the MOSR was kept at 75 psi and the flow rate was 0.7 gpm. Deoxygenating took place using N_2 and was maintained through out the entire experiment. The temperature was 25 $^{\circ}$ $\pm 3^{\circ}$C for all trials.

From Figure 21 it can be seen that the rate of ferrous iron oxidation is dependent on the ferrous iron concentration, as has been previously demonstrated. It is assumed that after a certain initial ferrous iron concentration the change in ferrous iron of the system remains constant. The change in ferrous iron remaining constant after a certain initial ferrous iron concentration was seen in the ILS system (Hustwit et al. 1992).

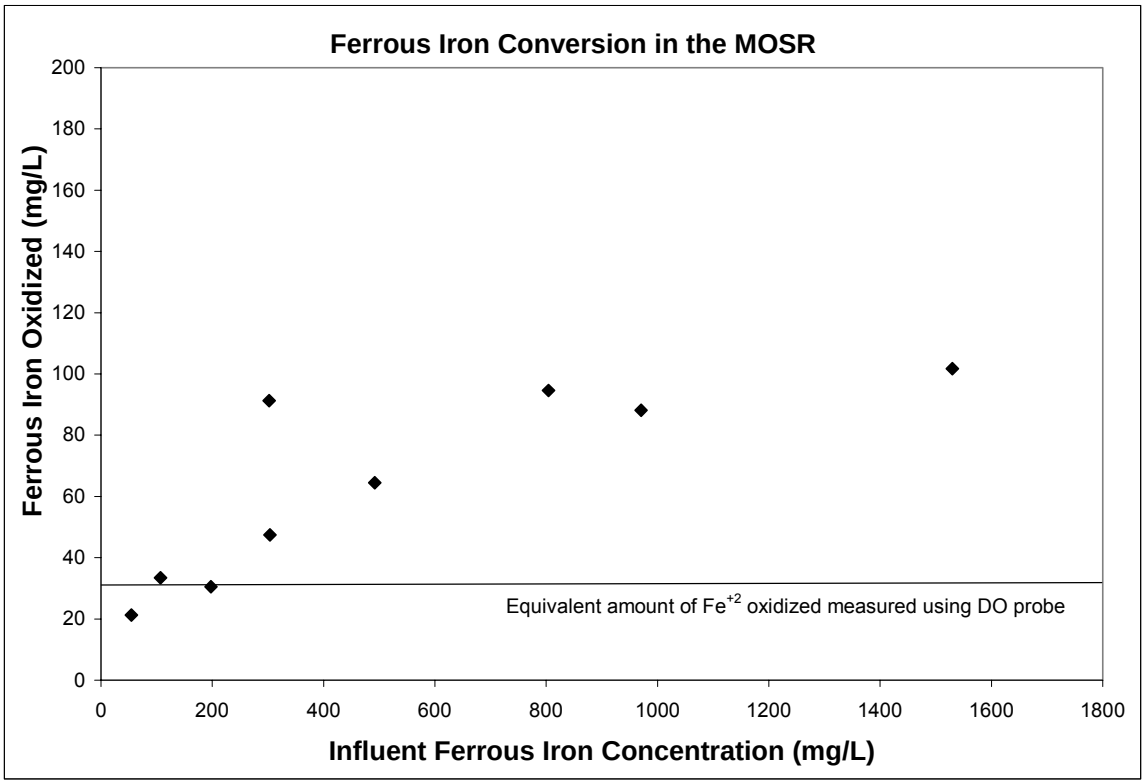

Figure 21 Ferrous iron oxidation as a function of concentration. P(psi) = 70, NaOH = 0.015 eq/L

In Figure 21 the measured MOSR change in ferrous iron is greater than can be explained by oxygen transfer as measured using a DO probe. As stated before this method is suitable for water where a very slow chemical reaction or none at all takes place with in the water. As a

result the O_2 gradient is not maximized. Therefore comparing the amount of ferrous iron that should be oxidized by relating the O_2 transferred as measured using a DO probe may not be entirely accurate.

It can also be argued that a reason for the ferrous iron oxidation being larger than the value of O_2 transferred may be due to the fact that cavitation takes place as the liquid flows through the orifices. The cavitation results in a vapor zone which enhances ferrous iron oxidation due to larger diffusivities of O_2 in the vapor phase.

The alternative to using a DO probe, deoxygenating with excess sulfite and then measuring the production of SO_4, may be thought of as a better method for measuring the oxidation ability of a system, but is still erroneous from a kinetic view point. In figure 17 the measured MOSR change in ferrous iron for all tests is less than the average value of ferrous iron that would be oxidized when the results of O_2 transfer measured using sulfate analysis (table 4) is stoichiometrically converted in to an equivalent amount of iron oxidized.

The problem with using the sulfate analysis method to measure oxygen transfer for this case are the kinetics of SO_3 oxidation are different than the kinetics of ferrous iron oxidation. The kinetics of Fe^{+2} oxidation are pH dependent. At a high pH the kinetics of Fe^{+2} oxidation are probably similar to the kinetics of sulfite oxidation, almost instantaneous. In the MOSR due to hydrolysis, one can assume the pH with in the reaction zone is driven down quite rapidly. Therefore, the mass transfer of oxygen into AMD with in the MOSR reaction zone is transient. Due to this state of transience it is difficult to compare the oxygen transfer results with the SO_4 measurements with the results of ferrous iron oxidation in the MOSR. The comparison of the two constituent oxidation rates becomes a kinetic evaluation. In order to model the mass transfer of oxygen within the MOSR when using AMD, any ferrous iron oxidation model applied to this particular situation would have to have its parameters updated after each time step. The main parameter requiring an update being the $[OH^-]$. Also in modeling this situation the mass transfer rate measurements would have to be adjusted to incorporate changes in rates due to chemical reactions.

4.4 NITROGEN EXPERIMENTS

By surrounding the MOSR with a blanket of N_2 the notion of the MOSR having an intrinsic oxidizing capability was to be investigated. This was done by sealing the MOSR in a plastic Tupperware© container. The container had a discharge hole for the effluent which was directed through a funnel. The container had an inlet for NaOH addition, an inlet for a gas dispersion tube, and a hole for gas to vent. A schematic of the experimental setup is shown in Figure 22.

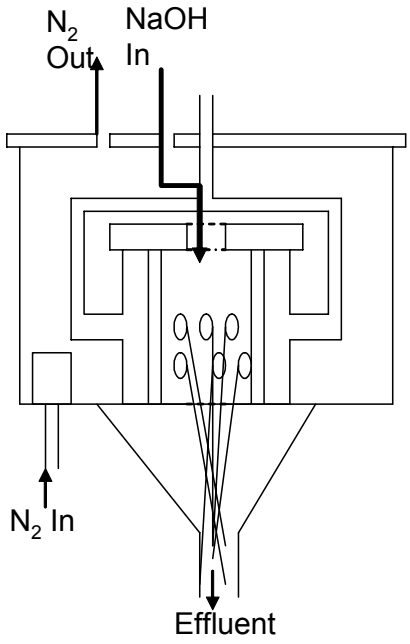

Figure 22 Schematic showing N_2 blanket around MOSR

To insure the container held gas the gas discharge vent was covered while N_2 was being discharged into the container. As a result of the pressure increase in the container the top of the container violently came off.

Table 6 shows the results of SO_3 oxidation taking place when the MOSR was surrounded by N_2. Between the two tests there was a minute change in SO_4, most likely due to experimental error. This says that the N_2 conditions around the MOSR prevent any oxidation taking place due to O_2 transfer or any other oxidation mechanism resulting from liquid flow through an orifice.

Table 6 Results of SO_3 oxidation in the presence of N_2 gas

Test 1

Inlet SO_4 Concentration (mg/L)	Outlet SO_4 Concentration (mg/L)	Equivalent Amount of O_2 Transferred (mg/L)
226.81	232.61	$0.99 \cong 0$
T('C) =22	**P(psi)=72**	**Q(gpm)= 0.7**

Test 2

Inlet SO_4 Concentration (mg/L)	Outlet SO_4 Concentration (mg/L)	Equivalent Amount of O_2 Transferred (mg/L)
223.91	226.09	$0.37 \cong 0$
T ('C) =19	**P(psi)=72**	**Q(gpm)=0.7**

The next test conducted was the oxidation of ferrous iron under the anoxic conditions. Table 7 shows the results of the ferrous iron experiments conducted in the presence of nitrogen at the MOSR outlet.

Table 7 Results of ferrous iron oxidation in the presence of N_2 gas. Q = 0.7 gpm, P = 73 psi, T=22-27°C

Fe^{+2} Concentration (mg/L)	Change in Absorbance (510 nm)	pH Initial	pH Final
311	0.04 ≅ 0	6.7	9.2
391	0.07 ≅ 0	5.9	11
752	0.05 ≅ 0	6.3	7.4
1051	0.10 ≅ 0	6	7.7
1632	0.04 ≅ 0	5.9	8
With No Inner Cylinder			
302	0.01≅ 0	6.2	7.3

The change in absorbance values shown in table 7 are approximately zero, therefore the changes in Fe^{+2} are not reported because a substantial change would be falsely reported due to factors relating to dilution. The decrease in absorbance may most likely be a result of experimental error.

Under anaerobic conditions at an operating pressure of 70 psi no oxidation is taking place in the MOSR.

4.5 IRON REMOVAL VERSUS OXIDATION

Active treatment of AMD generally oxidizes metals that are in the reduced form in order to make them less soluble at a lower pH value. The following section discusses the mechanism of iron removal, precipitation, within the bench scale MOSR setup.

Within the MOSR setup neutralization takes place by injecting NaOH into the suction side of the MOSR. When neutralization takes place in this manner, complete mixing of the NaOH and AMD stream does not take place until the liquid jets emanating from the discharge end of the MOSR meet in a sedimentation tank or beaker. Proof of this principle was presented through observation. When operating the MOSR system the liquid jets emanating from the MOSR remain colorless until they thoroughly mix with in a sampling container. Then a precipitate is almost immediately formed. Figure 23 describes this affect.

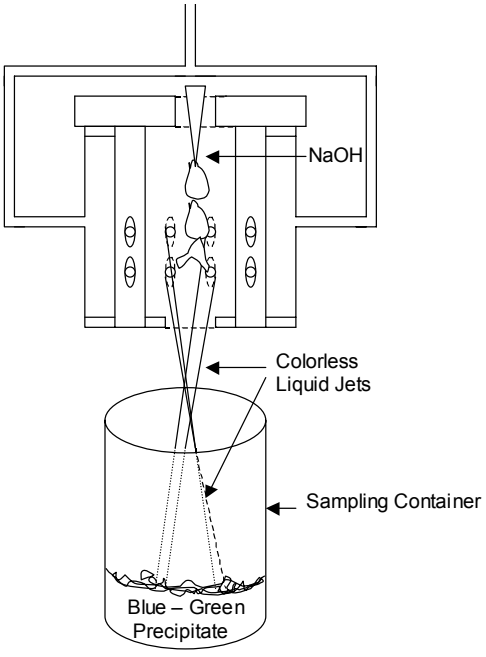

Figure 23 Schematic showing precipitate formation upon sampling

It is believed that the "instantaneous" precipitate of the MOSR is of the ferrous form due to the color of the precipitate. Upon collection from the MOSR the precipitate was noticed to have a blue-green hue. This color suggests ferrous iron. Lin et al. (1996) report that the formation of Green Rust II takes place in neutral or alkaline suspensions when $FeSO_4$ is used as the chemical to prepare the suspension. Green Rust contains both Fe^{+2} and Fe^{+3} although its chemical composition has not been exactly identified.

Another reason to believe that the precipitate formed immediately exiting the MOSR is of the ferrous form is because of the results of the following experiment. An experiment using the MOSR was conducted using St. Michael's AMD at 72 psi, 0.7 gpm, T $^{\circ}$C = 22, and NaOH concentration was varied and introduced at 150 mL/min. The samples were filtered using a 0.45 micron filter before adding acid. After filtration the samples were then acidified using concentrated HCL. Then the sample was analyzed for total iron using the Perkin Elmer flame atomic absorption unit. The results are shown in table 8. The results show that after analysis the total iron in solution when a concentration of 0.1 M NaOH was used was 16 mg/L. It has previously been shown that at 70 psi and 0.015 eq/L NaOH the MOSR can oxidize approximately 30% of the initial ferrous iron. These results suggest that under these conditions the majority of iron is precipitating as ferrous iron due to the insolubility resulting from the relatively high local pH. As the remaining soluble iron becomes insoluble the pH is subject to a decrease.

Table 8 Results of total iron concentrations of filtered MOSR effluents. Samples collected immediately exiting the MOSR.

Influent Fe^{+2} (mg/L)	NaOH (eq/L)	pH	MOSR Effluent: Soluble Fe (mg/L)
138	0.15	12.1	0.3
138	0.015	6.5	15.6
138	0.008	6.1	30
P(psi) = 70 Q(gpm) = 0.7 T (ºC) = 23 ºC			

Some of the precipitate formed initially is a ferrous and then converts to a ferric over time, as oxygen diffuses into solution and reacts with the solid ferrous hydroxides or oxides.

A third reason to believe that ferrous iron is precipitating is based on the equations and rate constants as reported by Wehrli (1990). The following stoichiometric constants and chemical equations are that of ferrous iron speciation at standard temperature and pressure.

$$Fe^{2+} + OH^- \rightarrow FeOH^+ \qquad k_1 = 10^{4.5} \qquad (19)$$

$$Fe^{2+} + 2OH^- \rightarrow FeOH_2 \qquad k_2 = 10^{7.4} \qquad (20)$$

A mass balance on ferrous iron yields:

$$Fe^{+2}{}_T = [Fe^{+2}] + [FeOH^+] + [Fe(OH)_2] \qquad (21)$$

By rearranging the above equations we arrive at

$$[Fe^{+2}] = Fe^{+2}_T/(1 + k_1[OH^-] + k_2[OH^-]^2) \quad (22)$$

$$[FeOH^+] = k_1\, Fe^{+2}_T[OH^-]/(1 + k_1[OH^-] + k_2[OH^-]^2) \quad (23)$$

$$[Fe(OH)_2] = k_2Fe^{+2}[OH^-]^2/(1 + k_1[OH^-] + k_2[OH^-]^2) \quad (24)$$

In order to gain an idea of the local pH inside the reaction zone a material balance on the reaction zone can be performed. For simplification purposes the buffer capacity of the water is not considered. At an AMD flow rate of 0.7 gpm and pH = 4.5 and a NaOH flow rate of 150 mL/min and concentration of 0.1 N the pH in the reaction zone approaches 11.7.

At a pH = 11.7, and a total ferrous iron concentration of 150 mg/L it can be shown that the Fe^{+2}, $FeOH^+$, and $Fe(OH)_2$ concentrations are as follows:

$[Fe^{+2}] = Fe^{+2}_T/(1 + k_1[OH^-] + k_2[OH^-]^2) = 0.003/(1+10^{4.5}(0.005)+10^{7.4}(0.005)^2) = 4E\text{-}6M = 0.2$ mg/L

$[FeOH^+]=k_1Fe^{+2}_T[OH^-]/(1+k_1[OH^-]+k_2[OH^-]^2)=$
$(10^{4.5}(0.003)(0.005))/(1+10^{4.5}(0.005)+10^{7.4}(0.005)^2) = 6E\text{-}4M = 33.8$ mg/L

$[Fe(OH)_2]=k_2Fe^{+2}[OH^-]_2/(1+k_1[OH^-]+k_2[OH^-]^2)=$
$(10^{7.4}(0.003)(0.005)^2)/(1+10^{4.5}(0.005)+10^{7.4}(0.005)^2) = 2.4E\text{-}3M = 134.4$ mg/L

The above approximations show that when the NaOH reacts with the AMD, assuming complete mixing takes place instantaneously, that 90% of the iron in the reaction zone of the MOSR or in the sampling container used to collect the samples from the MOSR is of the form $Fe(OH)_2$.

Based upon the content of the above sections there are two mechanisms taking place inside the MOSR. These mechanisms are oxidation of ferrous iron to ferric iron and precipitation of ferrous and ferric iron. A possible sequence of reactions for the precipitation and then oxidation of ferrous iron may be:

$$Fe^{+2} + 2H_2O \rightarrow Fe(OH)_2(s) + 2H^+ \quad (25)$$

$$Fe(OH)_2(s) + ½\ O_2 + H^+ \rightarrow Fe(OH)_3(s) \quad (26)$$

In the above set of equations, eq.28 usually happens at a pH > 8. The pH of the AMD and NaOH liquid reaches a value of around 11. Due to the minimum solubility of ferrous iron at pH 11 – 12, the Fe^{+2} precipitates out. Upon precipitation the Fe^{+2} undergoes hydrolysis and produces acidity. The acidity formed brings the pH down to the value reported in the experiments as final pH. This pH value is usually 6 – 9 depending on the experimental conditions. As the ferrous hydroxide remains in the sedimentation tank or sample beaker, oxygen diffuses from the atmosphere and oxidizes the ferrous hydroxide to ferric hydroxide. This is shown in equation 31.

Going back to the above hypothetical situation with an initial ferrous concentration of 150 mg/L the acidity produced in accord with equation 30 is in hydrogen to ferrous ion ratio of 2:1. Therefore at a ferrous concentration of approximately 0.003 M the hydrogen ion concentration due to hydrolysis is 2(0.003 M) = 0.006 M. The estimated OH^- concentration inside the reaction zone of the MOSR is approximately 0.005 M. This explains why the measured pH of the solution is near neutral at the time of pH measurement.

5.0 SUMMARY AND CONCLUSIONS

The multiple orifice spray reactor (MOSR), consisting of multiple orifices within an annulus, is an effective approach for the treatment of ferrous containing mine drainage. An investigation on the kinetics of the MOSR revealed the following:

- The experimental system is constrained by the physical limitations encountered in the lab. The operating pressure varied from 20 – 70 psi. In the MOSR flow rate was directly proportional to pressure.

- Images of the spray pattern in the inner cylinder of the MOSR showed that greater liquid surface area resulted as the pressure drop increased. The images also showed that inconsistencies in the spray patterns for each orifice were apparent. These inconsistencies should be avoided in order to better understand the MOSR process.

- The images of the sprays exiting the MOSR showed that the sprays in the inner cylinder of the MOSR collide, mix, and then produce a spray. The resulting spray has a unique droplet size distribution which greatly enhances the interfacial surface area of the liquid. As a result of this increased surface area, mass transfer of O_2 into the liquid phase is greater and hence rates of ferrous iron oxidation are greater.

- The oxygen transfer of the MOSR was evaluated. The results show that k_{La} increases as a function of pressure. It was also shown that all most all of the mass transfer takes place inside of the inner cylinder of the MOSR.

- The MOSR greatly increases ferrous iron oxidation rates above theoretical limits by relatively high mass transfer rates of oxygen due to multiple orifices. At an effluent pH of

6.5 the MOSR oxidizes ferrous iron to ferric iron at a rate about 4 orders of magnitude higher than theoretically predicted. These accelerated oxidation rates are likely due to increased interfacial surface area of the liquid flow within the multiple throats of the orifice reactor. Also, as the liquid flows through an orifice there also may be a vapor zone which increases oxidation rates as well. The vapor zone is due to the presence of cavitation as the liquid flows through the orifices. In addition, it is suggested that formation of $Fe(OH)_2$ in the reactor also results in subsequent increased ferrous iron oxidation rates.

- The rates of ferrous iron oxidation with in the MOSR increase as a function of pressure until 50 psi where the rates then begin to level off. The trend in data for ferrous iron oxidation as a function of pressure resembles the trend in data with k_{La} as a function of pressure. More data over a wider operating range is needed to differentiate the effects of oxygen transfer on oxidation from another oxidation mechanism such as cavitation.

- The rate of ferrous iron oxidation with respect to time taking place in the MOSR effluent is greatly increased as the liquid elements travel through the ambient air. Hence the oxidation is maximized as flight time of the spray is maximized. When the liquid collects in the sedimentation tank the rate of oxidation approaches zero. At this point the rate determining step is the diffusion of oxygen in to the bulk liquid as governed by Fick's Law.

- The rate of ferrous iron oxidation in the MOSR is much greater than in control samples which reflect conventional active treatment technologies.

- The amount of ferrous iron conversion immediately exiting the MOSR as a function of influent ferrous iron appears to reach a constant after an influent ferrous concnentration of 1000 mg/L. This asymptotic value represents the oxidation capability of the bench scale MOSR at 70 psi and a NaOH concentration of 0.015eq/L. The oxidation capability of the MOSR is 100 mg/L Fe^{+2}.

- A set of experiments conducted with the MOSR under a N_2 blanket show that the oxidation is not taking place in the absence of oxygen.

- Removal of iron in the MOSR is likely due to a high pH inside the reactor which precipitates ferrous iron.

In conclusion, the MOSR is an effective remediation technology for the treatment of acid mine drainage. Due to the MOSR's unique geometrical configuration there is an increased oxidation potential and hence ferrous iron oxidation. These increased rates are due to a larger surface area resulting from liquid flow through an orifice. There may also be some type of increased oxidation due to the effects of hydrodynamic cavitation, most likely a vapor phase reaction. The bench scale MOSR is physically limited due to its size. As a result of the flow limitations the bench scale MOSR is unable to fully oxidize AMD waters. This results in a large quantity of ferrous iron precipitation, which may re-dissolve as the pH of the effluent depresses due to hydrolysis. It is likely that larger scaled systems can produce greater oxidation differentials when the atomization and mixing of the AMD can be of a greater magnitude under field operating conditions.

6.0 RECOMMENDATIONS FOR FUTURE WORK

The recommendations for future work can be broken into two sections as follows: 1) study on enhancing the manageability of the products of the reaction and 2) study on enhancing the chemical reaction.

1) Enhancing the manageability of the products of the reaction.

Work needs to be completed on the settling rates of the sludge produced in this system. The process involves a local but temporal high pH which leads to the rapid precipitation of particles. This rapid precipitation of particles may also lead to the rapid agglomeration of particles and hence higher rates of settling as compared to conventional treatment processes. Also the settling rates produced when different alkaline agents are used for neutralization needs to be considered.

One major concern of today with AMD is the generation of large quantities of sludge. Many governmental agencies are looking for ways to reuse the sludge generated from acid mine drainage. Studies investigating the purity of sludge produced as a function of alkaline agent and mine water also need to be investigated. The reuse of sludge as an adsorbent in water treatment should be investigated. The particle size distributions of sludge produced from the MOSR process should be investigated in order to better characterize the products of this process.

2) Enhancing and modeling the chemical reaction kinetics in a MOSR

Can the MOSR be modeled in a similar manner to an absorption tower or scrubber? Work has been done on the modeling of spray towers where a gas is absorbed into the liquid phase and then a reaction takes place. Maybe the MOSR can be modeled as a plug flow reactor where a liquid element travels as a plug flow through an infinite volume of gas.

Maybe the MOSR can be used in conjunction with a strong oxidizing agent such as H_2O_2 or O_3. These reagents could be dispensed into the suction side of the MOSR as was done with the alkaline agent. This would facilitate oxidation at a lower pH value and precipitation of ferric iron would occur at acidic pH values. Neutralization would still be needed but perhaps the cost of neutralization would be less and a purer product may be formed.

With in a MOSR type system can the chemical effects of hydrodynamic cavitation be isolated? This would involve defining a proper operating range where cavitation is empirically or theoretically shown to exist. Once this is done the difference in oxidation from cavitation and oxygen transfer would need to be separated.

It is known that when flow enters a sharp edged orifice, the flow detaches from the sides of the orifice and forms a vena contracta. The contraction at the inlet sufficiently reduces the cross sectional area of the flow. This reduced flow area results in a localized increase in liquid velocity and subsequent pressure drop. If the absolute pressure falls below the vapor pressure of the liquid then cavitation results with vapor cavities forming with in the bulk fluid. Tseng and Collicott (2000) report that cavitation in an orifice is almost always present in flow through an orifice at and downstream of the inlet hole, and has been demonstrated from 4 psi to 30,458 psi (30 KPa to 210 MPa). As the pressure in the bulk liquid recovers, these cavities rapidly collapse. In the case of the MOSR, the recovered pressure (outlet) is approximately equal to atmospheric.

One way to asses the occurrence of cavitation in fluid flow through an orifice is through the use of Bernoulli's equation. From Bernoulli's equation, a dimensionless cavitation number, σ, can be derived which measures the resistance of flow to cavitation. The cavitation number, σ, is deduced from the relation between static pressure, P, and flow velocity, u. Bernoulli's equation states that the pressure drops due to flow are proportional to the product of fluid density and the square root of the flow velocity.

The cavitation number, σ, is obtained by dividing the available static pressure, $P_0 - P_v$, by the dynamic flow pressure (Shah et al. 1999):

$$\sigma = \frac{P_0 - P_v}{\frac{1}{2}\rho u^2} \qquad (27)$$

Where P_0 is the ambient pressure or pressure downstream of the orifice, P_v is the vapor pressure of the fluid flowing through the orifice, ρ is the liquid density, and u is the liquid velocity through the orifice. The particular value at which cavitation is incipient is termed the "cavitation inception number". Under ideal conditions, cavitation usually occurs for $\sigma < 1$, all though cavitation inception can occur at cavitation number values greater than and less than 1.

If the MOSR was designed for cavitation to take place, perhaps these effects could be better isolated. The presence of cavitation in such a reactor would be a function of the orifice diameters. Experiments need to be conducted using varying orifice diameters. In the bench scale MOSR at an orifice diameter of 0.032 in. (the current diameter) and a flow rate of 0.7 gpm there is a cavitation number of 5 and at an orifice diameter of 0.020 in and 0.7 gpm there is a cavitation number of 0.68. It should be noted that in the bench scale MOSR there is a visible difference in the spray patterns emanating from the orifices. These different spray patterns are most likely due to different orifice diameters. There fore the orifice diameter reported here should only be taken as an estimate.

When cavities collapse, localities of high temperature and pressure exist. These high temperatures and pressures can enhance chemical oxidation reactions. In addition, the generation of local high temperatures and pressures induces the cleavage of water molecules and results in the formation of free radicals such as OH*. Free radicals such as OH* have very strong oxidizing capabilities which may further oxidize ferrous iron. Strong oxidizing abilities generated by cavitiation was reported by Kumar et al. (2000), who used flow through an orifice plate to induce bacteria oxidation and inactivation.

Another question to be explored is, in the presence of cavitation can the vapor zone that is produced be shown to enhance rates of reactions where O_2 is the electron acceptor, and be accurately isolated from oxygen transfer. The diffusitives for a gas are orders of magnitudes

higher than diffusivities for liquids. This would enhance chemical reactions when the dissolved reactive species come into contact with the vapor region in a cavitating flow. By using the Rayleigh – Plesset equations describing bubble growth and the differential equations describing convective transport it is possible to model the extent and "volume" of a cavitating region given a set of boundary conditions. Then using this information on the vapor region and rates of diffusivity of liquids and gases (vapors) evaluate the kinetics of chemical reactions inside a cavitation zone of a particular reactor.

APPENDIX A

EXPERIMENTAL DATA

Table A 1 St. Michaels's mine water experimental oxidation rate

St. Michael's Mine Water Experimental Oxidation Rate.

1 L of St. M AMD was constantly aerated using a airstone.
DO was maintained at 8.9 - 9.3 mg/L throughout the experiment.
Temp. = 19.5 Celsius
pH was maintained at 6.2 allthough fluctuations occurred.
pH was always in the range of 6.1 - 6.4.
0.1 N NaOH

Time (sec.)	Time (min.)	Absorbance (510 nm)	[Fe2+] (mg/L)
0.00	0.00	0.51	124.46
100.00	1.67	0.23	55.97
300.00	5.00	0.09	21.48
450.00	7.50	0.06	14.63
800.00	13.33	0.02	5.33
1000.00	16.67	0.02	4.11

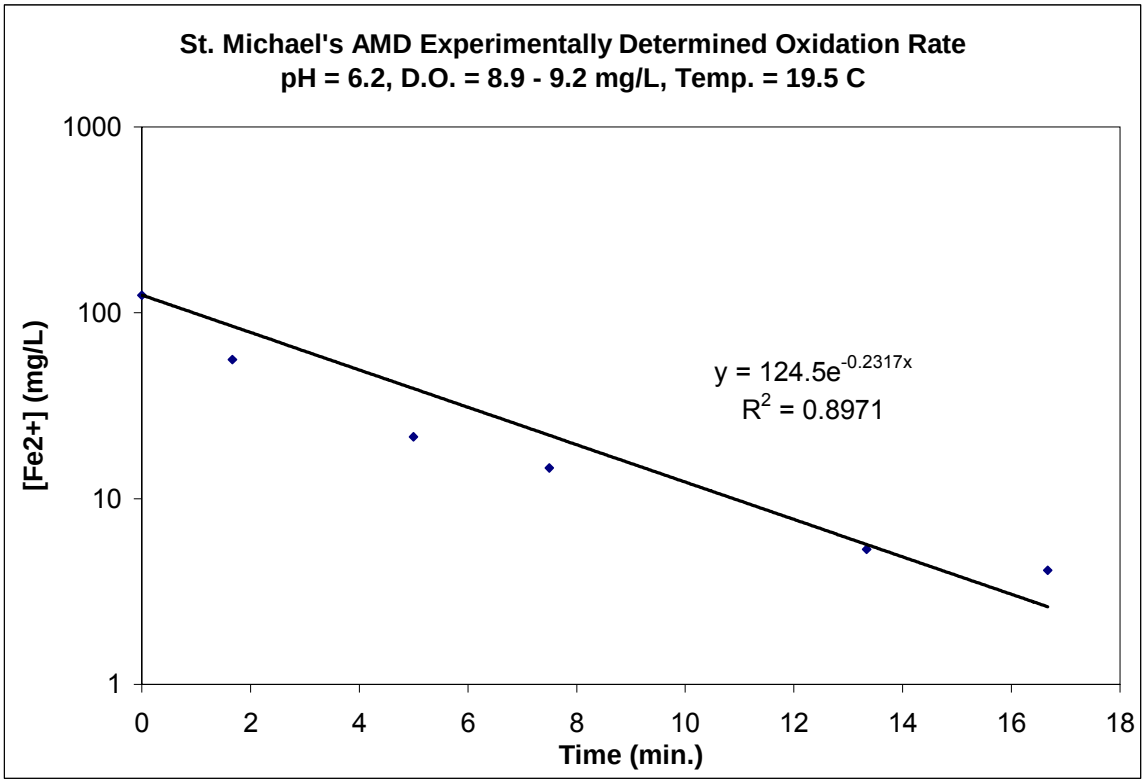

Figure A 1 St. Michael's mine water oxidation test procedure

Table A 2 Flow rate as a function of pressure in the MOSR experimental system

Pressure (PSI)	FlowRate (GPM)	Flow Rate (LPM)
0	1.1	4.2
20	0.3	1.1
30	0.4	1.4
40	0.5	1.7
49	0.5	1.9
61	0.6	2.1
70	0.6	2.3
78	0.7	2.5

Table A 3 Data showing measurement of O_2 transfer at 70 psi

Test 1
V = ~ 5 gal.
1.3g Na2SO3
T =23.2 C
Q = 0.72 gpm
P = 72 - 74 psi

A funnel with a plastic tube on the end was secured on the outlet of the MOSR.
The water level in the funnel was constant throughout the experiment. It was about
0.5" above the outlet of the MOSR. This was done to minimize turbulence from sampling a
hence any reaeration.
Sample2 was collected underneath the MOSR as described above.
Sample1 was collected inline at a sampling port 56" before MOSR.

Sample	DO1 (mg/L)	DO2(mg/L)	Change in DO(mg/L)
1	2.2	6.4	4.2
2	2.0	6.3	4.3
3	2.0	6.4	4.4
4	2.2	6.3	4.1
5	1.9	6.4	4.5
6	2.0	6.4	4.4
7	2.0	6.2	4.2
8	1.9	6.1	4.2
Average	2.0	6.3	4.3

All conditions were kept the same as above.
Except a glass stopper was used to seal the TJ.

Sample	DO1 (mg/L)	DO2(mg/L)	Change in DO(mg/L)
1	3.9	5.1	1.2
2	3.0	4.1	1.0
3	3.0	3.9	1.0
4	3.0	3.9	0.9
5	3.0	3.8	0.9
6	3.2	4.0	0.8
7	3.0	3.8	0.8
8	3.2	3.9	0.8
Average	3.1	4.1	0.9

Table A 4 Second test on O_2 transfer at 70 psi

Test 2

V = ~ 5 gal. DOzero = .60
1.3g Na2SO3
T =23.2 C
Q = 0.72 gpm
P = 72 - 74 psi

A 500 mL beaker was used to sample the MOSR discharge.
It was held directly underneath the MOSR, with the edge of the beaker being about 0.5 " above the outlet of the MOSR.

Sample1 was collected inline at a sampling port 56" before TJ.

Glass stopper was used to seal the MOSR.

Sample	DO1 (mg/L)	DO2(mg/L)	Change in DO(mg/L)
1	3.38	3.68	0.3
2	3.47	3.95	0.48
3	3.96	4.33	0.37
Average	3.603333	3.986667	0.383333

Same conditions as above w/ no stopper.

Sample	DO1 (mg/L)	DO2(mg/L)	Change in DO(mg/L)
1	4.84	8.96	4.12
2	3.99	8.81	4.82
3	3.8	8.36	4.56
4	3.99	8.67	4.68
Average	4.155	8.7	4.545

Table A 5 O_2 transfer using N_2 as the de - oxygenating agent

Oxygen transfer using N2

T C = 28

P (psi) = 70 - 75

Q(gpm) = 0.68

Sample	DO Initial (mg/L)	DO Final (mg/L)	Change in DO (mg/L)
1,1	2.19	6.48	4.29
1,2	1.6	6.27	4.67
1,3	1.7	6.18	4.48
1,4	1.42	6.19	4.77
			4.5525

Table A 6 k_{La} measurements in the bulk liquid

Bulk Liquid Kla measurement of TurboJet.

15 gllons of tap water was deoxygenated using 6 grams sodium sulfite and 0.3 grams of cobalt chloride, equaling 105.6 mg/L sodium sulfite. The deoxygenated water was recycled through the system for 2.1 hours. A sample was collected from the discharge of the turbojet 45 seconds after the experiment started. This sample had a DO of 7.22 mg/L.

From the slope of the graph Kla = 0.0003 sec^{-1} = 1.08 $hour^{-1}$.

Volume =	15	gal.
Water Temp.	19.8	C
Pressure	90	psi
Flow	0.27	gpm

Cs tap =	9.52
C0 =	0.85
(Cs-C0)	8.67
log(Cs-C0)	0.938019
ln(Cs-C0)	2.159869

Time(sec.)	D.O. (mg/L)	(Cs-Ct)	log(Cs-Ct)	ln(Cs-Ct)
0	0.85	8.67	0.938019	2.159869
300	2.01	7.51	0.87564	2.016235
600	2.9	6.62	0.820858	1.890095
900	3.75	5.77	0.761176	1.752672
1200	4.4	5.12	0.70927	1.633154
1500	5.15	4.37	0.640481	1.474763
1800	5.61	3.91	0.592177	1.363537
2100	6.01	3.51	0.545307	1.255616
2400	6.19	3.33	0.522444	1.202972
2700	6.25	3.27	0.514548	1.18479
3000	7.05	2.47	0.392697	0.904218
3300	7.25	2.27	0.356026	0.81978
3600	7.45	2.07	0.31597	0.727549
3800	7.45	2.07	0.31597	0.727549
4100	7.74	1.78	0.25042	0.576613
4400	7.79	1.73	0.238046	0.548121
4700	7.91	1.61	0.206826	0.476234
5000	7.98	1.54	0.187521	0.431782
5300	8.07	1.45	0.161368	0.371564
5600	8.05	1.47	0.167317	0.385262
5900	8.17	1.35	0.130334	0.300105
6200	8.2	1.32	0.120574	0.277632
6500	8.25	1.27	0.103804	0.239017
6800	8.36	1.16	0.064458	0.14842
7100	8.22	1.3	0.113943	0.262364
7400	8.8	0.72	-0.14267	-0.3285
7700	8.78	0.74	-0.13077	-0.30111

Table A 7 Calibration curve for SO_4 measurements

Sulfate Oxidation-Calibration Curve

Sulfate standards were prepared from 1000 mg/L SO4 Stock Solution. Each standard contained 5 ml HCHO.

SO_4 Concentration (mg/L)	Absorbance (450 nm)
70	0.75
50	0.54
30	0.31
10	0.06
Blank*	0
DI H_2O	0

*5 mL HCHO + 5mL DI H_2O

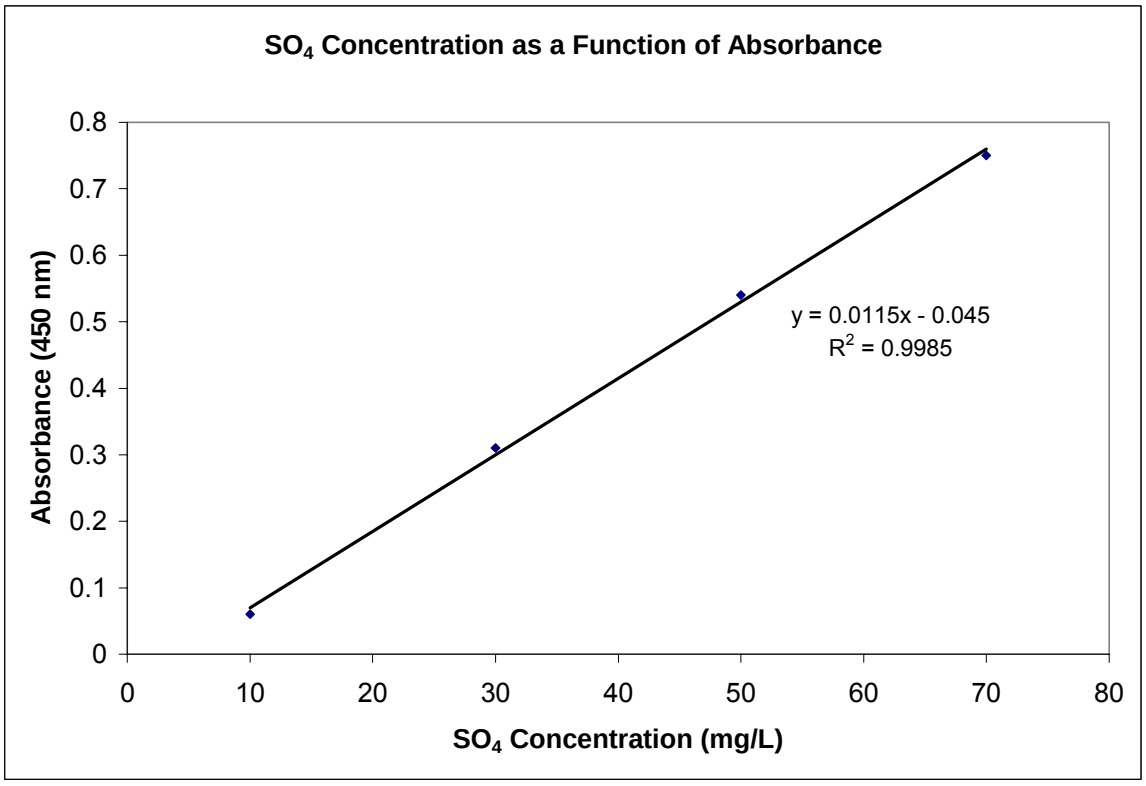

Figure A 2 SO_4 calibration curve

Table A 8 Data showing D.O. concentrations versus time with and with out HCHO

HCHO as a SO3 scavenger

4 g Na2SO3 + 5 mL 37% HCHO solution in 800 mL DI H2O
Aeration took place with an airstone.

Time (sec.)	DO (mg/L)
25	2.5
69	3.48
110	4.11
160	5.01
190	5.47
230	6.93
250	7.61
280	7.76
330	8.04
400	8.25

4 g Na2SO3 in 800 mL DI H2O
Aeration took place with an airstone.

Time (sec.)	DO (mg/L)
0	0.4
32	0.32
74	0.29
100	0.27
162	0.62
282	0.2
328	0.19
385	0.18
400	0.17

Table A 9 Results of SO_3 oxidation tests conducted on the MOSR

SO3 Oxidation - SO4 measured using HACH VERa4 SulfaPillows

5 mL HCHO/BOD bottle	T (C) =	22
10 g/L Na2SO3	P (psi) =	72
Dilution: 1mL sample/9 ml DI H2O	Q(gpm) =	0.68

Sample	Absorbance (450 nm)	SO4 Concentration (mg/L)	SO4 In Working Sample (mg/L)	Change in SO4 (mg/L)	Equivalent Amount of O2 Transferred (mg/L)
1,1	0.5	47	237	324	55
1,2	0.52	49	246	333	57
1,3	0.52	49	246	333	57
2,1	0.6	56	561		
2,2	0.62	58	578		
2,3	0.62	58	578		

pH 2-1	12.38	pH 1-1	12.42
pH 2-2	12.36	pH1-2	12.43
pH 2-3	12.32	pH1-3	12.37

SO3 Oxidation - SO4 measured using HACH VERa4 SulfaPillows

5 mL HCHO/BOD bottle	T (C) =	21.5
10 g/L Na2SO3	P (psi) =	74
Dilution: 1mL sample/9 ml DI H2O (set 2)	Q(gpm) =	0.7
2mL sample/8mL DI H2O (set 1)		

Sample	Absorbance (450 nm)	SO4 Concentration (mg/L)	SO4 In Working Sample (mg/L)	Change in SO4 (mg/L)	Equivalent Amount of O2 Transferred (mg/L)
1,1	0.5	47	237	80	14
1,2	0.5	47	237	228	39
1,3	0.52	49	246	141	24
2,1	0.32	32	317		
2,2	0.49	47	465		
2,3	0.4	39	387		

pH 2-1	12.45	pH 1-1	12.42
pH 2-2	12.45	pH1-2	12.39
pH 2-3	12.43	pH1-3	12.35

Table A 10 Data for typical ferrous iron calibration curve

Typical Fe+2 Calibration Curve

Concentration (mg/L)	Absorbance (510 nm)
0.02	0.0025
0.05	0.01
0.1	0.018
0.2	0.04
0.3	0.061
0.4	0.0833
0.5	0.1033
1	0.195
2	0.41
3	0.62
4	0.84
5	1.05
7	1.4

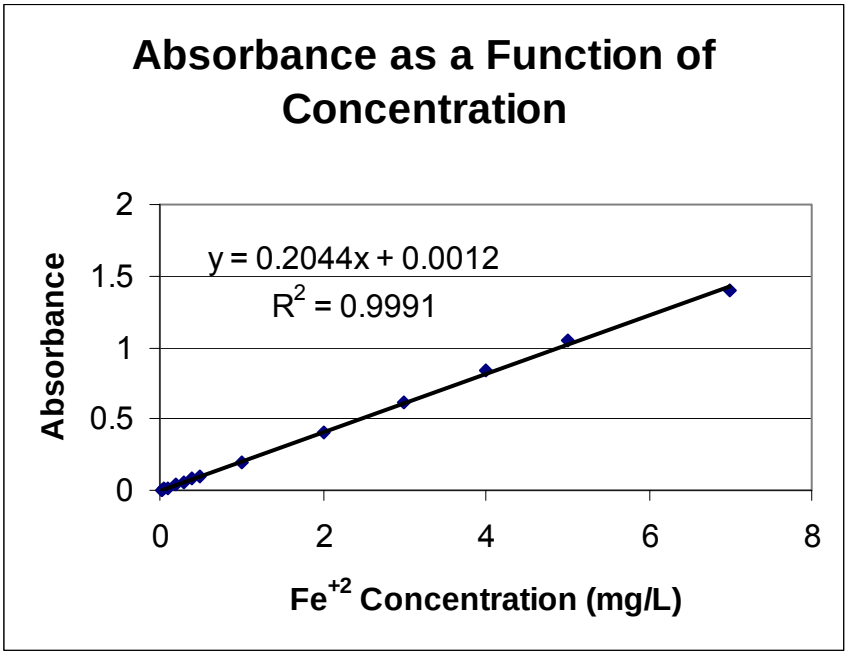

Figure A 2 Ferrous iron calibration curve

Table A 11 St. Michael's mine water oxidation tests

Trial 1 - St. Michaels AMD

Temp. (C')	22	DO initial (mg/	5.59
Q(TJ) (gpm)	0.72	DO final (mg/L	2.9
P (psi)	78	pH initial	4.6
Time (sec.)	235	pH final	6.4

Caustic	
0.1	M NaOH
150	mL/min

Sample	Abs	Concentration in Working Sample (mg/L)	Concentration after Adjustment (mg/L)	Oxidation Rate (mg/L-min)
1,1	0.52	2.54	126.91	5283.76
2,1	0.54	2.64	131.80	5577.30
3,1	0.54	2.64	131.80	5591.98
1,2	0.16	0.78	38.85	
2,2	0.16	0.78	38.85	
3,2	0.159	0.77	38.60	
Percent Reduction			70.22	5484.34

Sludge Production

Sludge was formed instantly. It was reddish/yellow in color. It was very "fluffy" and seemed to settle poorly.

TableA11(continued).

Trial 2 - St. Michaels AMD

Temp. (C')	22	DO initial (mg/	5.9
Q(TJ) (gpm)	0.72	DO final (mg/L	1.96
P (psi)	75	pH initial	4.6
Time (sec.)	266	pH final	9.5

Caustic	
0.2	M NaOH
150	mL/min

Sample	Abs	Concentration in Working Sample (mg/L)	Concentration after Adjustment (mg/L)	Oxidation Rate (mg/L-min)
1,1	0.52	2.54	126.91	6237.77
2,1	0.54	2.64	131.80	6531.31
3,1	0.539	2.63	131.56	6457.93
1,2	0.095	0.46	22.95	
2,2	0.095	0.46	22.95	
3,2	0.099	0.48	23.92	
Percent Reduction			82.11	6409.00

Sludge Production

Sludge was formed instantly. It was a blue/green color.

After sitting in a beaker open to the atmosphere, sludge turns dark brown and slowly to red.

Table A 11 (continued).

Temp. (C')	22	DO initial (mg/	5.9
Q(TJ) (gpm)	0.72	DO final (mg/L	1.45
P (psi)	75	pH initial	4.6
Time (sec.)	266	pH final	8.28

Caustic	
0.15	M NaOH
150	mL/min

Sample	Abs	Concentration in Working Sample (mg/L)	Concentration after Adjustment (mg/L)	Oxidation Rate (mg/L-min)
1,1	0.5	2.44	122.02	5944.23
2,1	0.51	2.49	124.46	6164.38
3,1	0.51	2.49	124.46	6127.69
1,2	0.095	0.46	22.95	
2,2	0.09	0.43	21.72	
3,2	0.0925	0.45	22.33	
Percent Reduction			81.94	6078.77

Sludge Production

Sludge was formed instantly. It was a blue/green color. After sitting in a beaker open to the atmosphere sludge turns dark brown and slowly to red.

Table A 11 (continued).

Trial 4 - St. Michaels AMD

Temp. (C')	22	DO initial (mg/	5.76
Q(TJ) (gpm)	0.72	DO final (mg/L	2.75 - 3.34
P (psi)	72	pH initial	4.17
Time (sec.)	204	pH final	5.59

Caustic	
0.05	M NaOH
150	mL/min

Sample	Abs	Concentration in Working Sample (mg/L)	Concentration after Adjustment (mg/L)	Oxidation Rate (mg/L-min)
1,1	0.48	2.34	117.12	2935.42
2,1	0.51	2.49	124.46	3375.73
3,1	0.51	2.49	124.46	3375.73
1,2	0.28	1.36	68.20	
2,2	0.28	1.36	68.20	
3,2	0.28	1.36	68.20	
Percent Reduction			44.11	3228.96

Sludge Production

First the solution was a light green then it went to yellow.
The sludge formed was almost instantly a yellow red.

Table A 11 (continued).

Trial 5 - St. Michaels AMD

Temp. (C')	22	DO initial (mg/	4.04
Q(TJ) (gpm)	0.74	DO final (mg/L	0.9
P (psi)	74	pH initial	3.75
Time (sec.)	204	pH final	7.56

Caustic	
0.125	M NaOH
150	mL/min

Sample	Abs	Concentration in Working Sample (mg/L)	Concentration after Adjustment (mg/L)	Oxidation Rate (mg/L-min)
1,1	0.5	2.44	122.02	6017.61
2,1	0.49	2.39	119.57	5973.58
3,1	0.5	2.44	122.02	6061.64
1,2	0.09	0.43	21.72	
2,2	0.083	0.40	20.01	
3,2	0.087	0.42	20.99	
Percent Reduction			82.75	6017.61

Sludge Production

First the solution was a light green then it went to yellow.
The sludge formed was almost instantly a deep brown and slowly turned red.

Table A 11 (continued).

Trial 6 - St. Michaels AMD

Temp. (C')	22	DO initial (mg/	6.2
Q(TJ) (gpm)	0.7	DO final (mg/L	8.32
P (psi)	74	pH initial	3.85
Time (sec.)	271	pH final	4.6

Caustic	
0.025	M NaOH
150	mL/min

Sample	Abs	Concentration in Working Sample (mg/L)	Concentration after Adjustment (mg/L)	Oxidation Rate (mg/L-min)
1,1	0.51	2.49	124.46	440.31
2,1	0.51	2.49	124.46	513.70
3,1	0.51	2.49	124.46	513.70
1,2	0.48	2.34	117.12	
2,2	0.475	2.32	115.90	
3,2	0.475	2.32	115.90	
Percent Reduction			6.55	489.24

Sludge Production

No sludge production was noticed. Solution remained clear with a yellow tint.

Table A 11 (continued).

Trial 7 - St. Michaels AMD

6/22/2004

Temp. (C')	25	DO initial (mg/	4.5
Q(TJ) (gpm)	0.7	DO final (mg/L	0.8
P (psi)	74	pH initial	5.2
Time (sec.)		pH final	6.23

Caustic	
0.1	M NaOH
150	mL/min

Sample	Abs	Concentration in Working Sample (mg/L)	Concentration after Adjustment (mg/L)	Oxidation Rate (mg/L-min)
1,1	0.56	2.73	136.69	5430.53
2,1	0.54	2.64	131.80	5577.30
3,1	0.56	2.73	136.69	6017.61
1,2	0.19	0.92	46.18	
2,2	0.16	0.78	38.85	
3,2	0.15	0.73	36.40	
Percent Reduction			70.03	5675.15
Filtered then Acidified				
3,3	0.065	0.31	15.61	
Percent Reduction			88.44	

Sludge Production

300 mL of water was collected and aloowed to settle for 2 hours. The volume of sludge settled equaled 25 mL. Overnight the volume of sludge equaled about 18 mL. Supernatant was very clear to the eye.

Table A 11 (continued).

Trial 8 - St. Michaels AMD

Temp. (C')	25	DO initial (mg/	5.4
Q(TJ) (gpm)	0.7	DO final (mg/L	0.2
P (psi)	74	pH initial	4.8
Time (sec.)		pH final	6.25

Caustic	
0.1	M NaOH
150	mL/min

Sample	Abs	Concentration in Working Sample (mg/L)	Concentration after Adjustment (mg/L)	Oxidation Rate (mg/L-min)
1,1	0.52	2.54	126.91	391.39
2,1	0.51	2.49	124.46	366.93
3,1	0.52	2.54	126.91	415.85
1,2	0.36	1.76	87.77	
2,2	0.36	1.76	87.77	
3,2	0.35	1.71	85.32	
Percent Reduction			31.04	391.39

Table A 12 Condensed results of St. Michael's mine water tests

Trial #	D.O. Concentration Initial (mg/L)	pH Initial	Ferrous Iron Concentration Initial (mg/L)	pH Final	Ferrous Iron Concentration Final (mg/L)	Normality of NaOH (eq/L)
1	6.2	3.85	124.46	4.6	116.31	0.025
2	5.76	4.17	122.01	5.59	68.2	0.05
3	5.59	4.6	130.17	6.4	38.77	0.1
4	4.04	3.75	121.2	7.56	20.91	0.125
5	5.9	4.6	123.24	8.28	22.33	0.15
6	5.9	4.6	130.09	9.5	23.44	0.2
*All tests were conducted at 20 C, 72 psi, and 0.7 gpm.						

Table A 13 Comparison of MOSR oxidation rate to theory

Trial #	Final pH	TJ Ferrous Iron Oxidation Rate (mg/L*min)	Iron Dependent Model Oxidation Rate (mg/L*min)
1	4.6	489.24	1.69E-04
2	5.59	3228.96	1.69E-02
3	6.4	5484.34	6.72E-01
4	7.56	6017.61	1.69E+02
5	8.28	6078.77	4.24E+03
6	9.5	6409.00	1.07E+06
* Iron dependent model based on K = 3.0E-12 mol/L*min at 20 C. DO = 8.7 mg/L. [Fe2+] = 130 mg/L.			

Table A 14 Caustic addition as a function of flow rate

Pressure (PSI)	FlowRate (GPM)	Flow Rate (LPM)	Volume of Flow in 1 Minute (L)	Standardized Volume of NaOH added in 1 minute (mL)	Concentration of NaOH (M)
0	1.10	4.16	4.16	150.00	0.17
20	0.30	1.14	1.14	150.00	0.05
30	0.38	1.44	1.44	150.00	0.06
40	0.45	1.70	1.70	150.00	0.07
49	0.50	1.89	1.89	150.00	0.08
61	0.55	2.08	2.08	150.00	0.08
70	0.60	2.27	2.27	150.00	0.09
78	0.66	2.50	2.50	150.00	0.10

Table A 15 Ferrous iron oxidation tests as a function of pressure

P (psi) = 20 psi

Temp. (C')	19.5	DO initial (	0.66
Q(TJ) (gpn	0.3	DO final (n	0.1
P (psi)	20	pH initial	6
Time (sec.)		pH final	8.24

Caustic	
0.045455	M NaOH
150	mL/min

Sample	Abs	Concentration in Working Sample (mg/L)	Concentration after Adjustment (mg/L)
1,1	0.58	2.83	141.59
2,1	0.59	2.88	144.03
3,1	0.58	2.83	141.59
1,2	0.365	1.78	88.99
2,2	0.375	1.83	91.44
3,2	0.35	1.71	85.32
	Percent Reduction		37.79

P (psi) = 30 psi

Temp. (C')	19.5	DO initial (	6.6
Q(TJ) (gpm)		DO final (n	0.33
P (psi)	30	pH initial	0.06
Time (sec.)		pH final	9

Caustic	
0.057576	M NaOH
150	mL/min

Sample	Abs	Concentration in Working Sample (mg/L)	Concentration after Adjustment (mg/L)
1,1	0.56	2.73	136.69
2,1	0.565	2.76	137.92
3,1	0.565	2.76	137.92
1,2	0.32	1.56	77.98
2,2	0.32	1.56	77.98
3,2	0.32	1.56	77.98
Percent Reduction			43.29

Table A 15 (continued).

P (psi) = 40 psi

Temp. (C')	19.5	DO initial (	0.7
Q(TJ) (gpn	0.45	DO final (n	0.1
P (psi)	40	pH initial	6
Time (sec.)		pH final	8.28

Caustic	
0.068182	M NaOH
150	mL/min

Sample	Abs	Concentration in Working Sample (mg/L)	Concentration after Adjustment (mg/L)
1,1	0.58	2.83	141.59
2,1	0.58	2.83	141.59
3,1	0.58	2.83	141.59
1,2	0.345	1.68	84.10
2,2	0.34	1.66	82.88
3,2	0.33	1.61	80.43
	Percent Reduction		41.75

P (psi) = 50 psi

Temp. (C')	19.5	DO initial (	0.7
Q(TJ) (gpm)		DO final (n	0.05
P (psi)	50	pH initial	6.65
Time (sec.)		pH final	9.3

Caustic	
0.075758	M NaOH
150	mL/min

Sample	Abs	Concentration in Working Sample (mg/L)	Concentration after Adjustment (mg/L)
1,1	0.58	2.83	141.59
2,1	0.57	2.78	139.14
3,1	0.59	2.88	144.03
1,2	0.34	1.66	82.88
2,2	0.33	1.61	80.43
3,2	0.33	1.61	80.43
	Percent Reduction		42.62

Table A 15 (continued).

P (psi) = 60 psi

Temp. (C')	19.5	DO initial (	0.58
Q(TJ) (gpn	0.55	DO final (n	0.1
P (psi)	60	pH initial	6.2
Time (sec.)		pH final	8.8

Caustic	
0.083333	M NaOH
150	mL/min

Sample	Abs	Concentration in Working Sample (mg/L)	Concentration after Adjustment (mg/L)
1,1	0.585	2.86	142.81
2,1	0.585	2.86	142.81
3,1	0.59	2.88	144.03
1,2	0.35	1.71	85.32
2,2	0.38	1.85	92.66
3,2	0.38	1.85	92.66
	Percent Reduction		37.01

P (psi) = 80 psi

Temp. (C')	19.5	DO initial (	0.7
Q(TJ) (gpm)		DO final (n	0.04
P (psi)	80	pH initial	6.65
Time (sec.)		pH final	9.4

Caustic	
0.1	M NaOH
150	mL/min

Sample	Abs	Concentration in Working Sample (mg/L)	Concentration after Adjustment (mg/L)
1,1	0.56	2.73	136.69
2,1	0.58	2.83	141.59
3,1	0.58	2.83	141.59
1,2	0.35	1.71	85.32
2,2	0.34	1.66	82.88
3,2	0.37	1.80	90.22
	Percent Reduction		38.45

Table A 16 Oxygen transfer tests as a function of pressure

Oxygen Transfer as a Funtion of Pressure

Temp. ('C) 23.5

P = 50 psi

Sample	DO (mg/L)	Average DO (mg/L)	Change in DO (mg/L)
1-1	1.24	1.04	4.51
1-2	0.95		
1-3	0.94		
2-1	5.33	5.55	
2-2	5.15		
2-3	6.17		

P = 30 psi

Sample	DO (mg/L)	Average DO (mg/L)	Change in DO (mg/L)
1-1	0.99	0.91	4.95
1-2	0.79		
1-3	0.94		
2-1	5.61	5.85	
2-2	5.94		
2-3	6.01		

P = 20 psi

Sample	DO (mg/L)	Average DO (mg/L)	Change in DO (mg/L)
1-1	0.95	0.96	4.20
1-2	0.96		
2-1	5.18	5.16	
2-2	5.13		

P = 60 psi

Sample	DO (mg/L)	Average DO (mg/L)	Change in DO (mg/L)
1-1	2.77	2.29	4.45
1-2	2.41		
1-3	1.68		
2-1	6.81	6.73	
2-2	6.71		
2-3	6.68		

Table A16 (continued).

P = 40 psi

Sample	DO (mg/L)	Average DO (mg/L)	Change in DO (mg/L)
1-1	1.46	1.42	4.98
1-2	1.39		
1-3	1.41		
2-1	6.43	6.40	
2-2	6.35		
2-3	6.43		

Table A 17 Ferrous iron oxidation as a function of initial ferrous iron concentration

Oxidation as a function of ferrous iron concentration

300 mg/L

TJ Flow	0.7	gpm
Pressure	72	psi
Caustic	0.1	N
Temperature	17.5	°C
CausticFlow	140ml/min	
pH Final	6.8	
Dilution	0.5mL/100mL	

Sample	Absorbance (510nm)	Concentration Working Sample (mg/L)	Concentration Sample (mg/L)	Change in Concentration (mg/L)
1,1	0.32	1.56	311.9373777	91.32420091
1,2	0.31	1.51	302.1526419	
1,3	0.3	1.46	292.3679061	
2,1	0.25	1.22	243.444227	
2,2	0.2	0.97	194.5205479	
2,3	0.2	0.97	194.5205479	

Table A17 (continued).

800 mg/L

TJ Flow	0.7	gpm
Pressure	78	psi
Caustic	0.1	N
Temperature	23.5	°C
CausticFlow	150	mL/min
pH Final	6.35	
Dilution	0.5mL/100mL	

Sample	Absorbance (510 nm)	Concentration Working Sample (mg/L)	Concentration Sample (mg/L)	Change in Concentration (mg/L)
1,1	0.82	4.01	801	95
1,2	0.8	3.91	782	
1,3	0.85	4.15	831	
2,1	0.71	3.47	694	
2,2	0.74	3.61	723	
2,3	0.73	3.57	713	

1050 mg/L

TJ Flow	0.6	gpm
Pressure	78	psi
Caustic	0.1	N
Temperature	22.2	°C
CausticFlow	150	mL/min
pH Final	6.2	
Dilution	0.2mL/100mL	

Sample	Absorbance (510 nm)	Concentration Working Sample (mg/L)	Concentration Sample (mg/L)	Change in Concentration (mg/L)
1,1	0.98	4.79	958	78
1,2	1	4.89	977	
1,3	1	4.89	977	
2,1	0.91	4.45	889	
2,2	0.9	4.40	879	
2,3	0.93	4.54	909	

Table A17 (continued).

1050 mg/L

TJ Flow	0.6	gpm
Pressure	78	psi
Caustic	0.1	N
Temperature	22.2	°C
CausticFlow	150	mL/min
pH Final	6.2	
Dilution	0.2mL/100mL	

Sample	Absorbance (510 nm)	Concentration Working Sample (mg/L)	Concentration Sample (mg/L)	Change in Concentration (mg/L)
1,1	0.64	3.13	1563	114
1,2	0.66	3.22	1612	
1,3	0.64	3.13	1563	
2,1	0.6	2.93	1465	
2,2	0.6	2.93	1465	
2,3	0.6	2.93	1465	

50 mg/L

TJ Flow	0.7	gpm
Pressure	76	psi
Caustic	0.1	N
Temperature	24	°C
CausticFlow	140	mL/min
pH Final	10.04	
Dilution	2mL/100mL	

Sample	Absorbance (510 nm)	Concentration Working Sample (mg/L)	Concentration Sample (mg/L)	Change in Concentration (mg/L)
1,1	0.225	1.09	55	21
1,2	0.225	1.09	55	
1,3	0.225	1.09	55	
2,1	0.139	0.67	34	
2,2	0.139	0.67	34	
2,3	0.136	0.66	33	

Table A17 (continued).

100 mg/L

TJ Flow	0.7	gpm
Pressure	76	psi
Caustic	0.1	N
Temperature	24	°C
CausticFlow	150	ml/min
pH Final	8.6	
Dilution	2mL/100mL	

Sample	Absorbance (510 nm)	Concentration Working Sample	Concentration Sample	Change in Concentration (mg/L)
1,1	0.44	2.15	107	33
1,2	0.435	2.12	106	
1,3	0.435	2.12	106	
2,1	0.29	1.41	71	
2,2	0.3	1.46	73	
2,3	0.31	1.51	76	

300 mg/L

TJ Flow	.7 gpm	gpm
Pressure	76 psi	psi
Caustic	.1 M	N
Temperature	22 °C	°C
CausticFlow	150	mL/min
pH Final	6.8	
Dilution	2mL/100mL	

Sample	Absorbance (510 nm)	Concentration Working Sample	Concentration Sample	Change in Concentration (mg/L)
1,1	0.62	3.03	303	47
1,2	0.625	3.05	305	
1,3	0.62	3.03	303	
2,1	0.527	2.57	257	
2,2	0.52	2.54	254	
2,3	0.527	2.57	257	

Table A17 (continued).

	500	mg/L
TJ Flow	0.7	gpm
Pressure	76	psi
Caustic	0.1	N
Temperature	22	°C
CausticFlow	150	mL/min
pH Final	6.67	

Dilution 2mL/100mL

Sample	Absorbance (510 nm)	Concentration Working Sample	Concentration Sample	Change in Concentration (mg/L)
1,1	1.04	5.08	508	64
1,2	1.03	5.03	503	
1,3	0.95	4.64	464	
2,1	0.865	4.23	423	
2,2	0.88	4.30	430	
2,3	0.88	4.30	430	

Table A 18 Data showing ferrous iron oxidation in MOSR effluent as a function of time

MOSR
First sample was collected initially after MOSR with acid.
Remaining samples were taken from a 1 L beaker.The beaker was kept mixed.

Q (gpm) = 0.7
P(psi) = 64

Q_{NaOH} (mL/ 150

Time (sec.)	Abs. (510 nm)	Fe2+ Concentration in Working Sample (mg/L)	Fe2+ Concentration (mg/L)	DO (mg/L)	pH
0	0.87	4.3	212.5	NA	6.96
2	0.725	3.5	177.1	NA	6.96
10	0.52	2.5	126.9	NA	7.00
90	0.25	1.2	60.9	0.46	6.96
120	0.24	1.2	58.4	0.36	6.96
185	0.22	1.1	53.5	0.25	7.01
255	0.22	1.1	53.5	0.20	7.04
310	0.21	1.0	51.1	0.17	7.05
410	0.2	1.0	48.6	0.14	7.04
695	0.16	0.8	38.8	0.12	6.89
Sampling Plane B	0.52	2.5	126.9		
Sampling Plane B	0.64	3.1	156.3		
Average				0.24	6.99
Standard Deviation				0.12	0.05

Table A 19 Ferrous iron oxidation as a function of time in control samples

Beaker was aerated with an air stone and mixed.
The amount of NaOH used was the same amount as
1L of water flowing through theMOSR would receive (82.425 mL).

Time (sec.)	Abs. (510 nm)	Fe2+ Concentration in Working Sample (mg/L)	Fe2+ Concentration (mg/L)	pH	DO (mg/L)
0	0.95	4.64	232.1	**7.30**	**9.50**
90	0.725	3.54	177.1	6.10	8.00
120	0.6	2.93	146.5	6.20	4.00
170	0.35	1.71	85.3	6.40	3.84
215	0.27	1.32	65.8	6.30	5.91
271	0.11	0.53	26.6	6.50	5.45
300	0.03	0.14	7.0	7.03	7.04
350	0.01	0.04	2.2	7.00	8.05
Average				6.60	6.47
Std. Dev.				0.44	2.03

BIBLIOGRAPHY

Ackman, T.E., and Kleinmann, R.L.P. (1984) "In Line Aeration and Treatment of Acid Mine Drainage" US Bureau of Mines, Report of Investigations 8868.

Ackman, Terry E., and Place, John M. (1987) Acid Mine Water Aeration and Treatment System. U.S. Patent No. 4,695,378.

APHA, AWWA, WPCF, (1998) Standard Methods for the Examination of Water and Wastewater. 20th Ed., Washington, D.C.

Clarke, L. B. (1995) Coal Mining and water quality. IEA Coal Research. London, UK, 99 pp.

Gogate, G. R., and Pandit, A. B. (2000) "Engineering Design Methods for Cavitation Reactors II: Hydrodynamic Cavitation" Journal of American Institute of Chemical Engineering. 46: 1641 -1649.

Hedin, R.S. and Nairn, R.W. 1992. Designing and sizing passive mine treatment systems. U.S. Bureau of Mines, Pittsburgh Research Center, Pittsburgh, USA

Hustit, C.C., Ackman, T.E., Erickson, P.M. (1992) "Role of Oxygen Transfer in Acid Mine Drainage Treatment" US Bureau of Mines, Report of Investigations 9405.

Hustwit, C.C., Ackman, T.E., Erickson, P.E. (1992) "The role of oxygen transfer in acid mine drainage (AMD) treatment" Water Environment Research. September/October

Kolbash, Ronald L. and Donald Budeit. (1988) "New Lower Cost Method for Treating Acid Mine Drainage: A Case History – Martinka Mine No. 1" Proceedings – 49th International Water Conference, Engineers Society of Western Pennsylvania. 398 – 92.

Kumar, P., Kumar, M., Pandit, A.B. (2000) "Experimental quantification of chemical effects of hydrodynamic cavitation" Chemical Engineering Science. 55:1633-1639.

Liang and Kester (1961) Oxygenation of Ferrous Iron. Ind. Eng. Chem., 53,143.

Lin, R., Spicer, R. L., Tungate, F. L., Davis, B. H. (1996) "A study of the oxidation of ferrous hydroxide in slightly basic solution to produce ϒ - FeOOH" Colloids and Surfaces A. 113: 79 – 96.

Metcalf & Eddy. (2003) Wastewater Engineering, Treatment and Reuse. McGraw-Hill Companies, Inc. New York, NY, 1819 pp.

Rossman, W., Wytovich, E., Seif, J. (1997) "Abandoned Mines – Pennsylvania's Single Biggest Water Pollution Problem.": n. pag. Online. Internet. Available: http://www.dep.state.pa.us/dep/DEPUTATE/MINRES/BAMR/MINING_01239htm

Shah, Y.T. (1979) Gas – Liquid – Solid Reactor Design. McGraw-Hill Inc. 373 pp.

Shah, Y.T., Pandit, A.B., Moholkar, V.S., (1999) Cavitation Reaction Engineering. Kluwer Academic/Plenum Publishers. New York, N.Y. 1999. 352 pp.

Smith, William H. and Werner, Roy H. (1984) Mixing Apparatus. U.S. Patent No. 4,74,477.

Stumm, W., and Lee, F.G. (1961) Oxygenation of Ferrous Iron. Ind. Eng. Chem., 53, 143.

Stumm, W., and Morgan, J., (1996) Aquatic Chemistry Chemical Equilibria and Rates in Natural Waters. John Wiley & Sons, Inc. New York, NY, 1022 pp.

Sung, W., and Morgan, J.J. (1980) Kinetics and Product of Ferrous Iron Oxygenation in Aqueous Systems. Environ. Sci. Technol., 14, 561.

Tamura, H., Goto, K., and Nagayama, M. (1976) The Effect of Ferric Hydroxide on the Oxygenation of Ferrous Ions in Neutral Solutions. Corr. Sci., 16, 197.

Toland, Bill. "Mine Reclamation Could Be A Mother Lode." (2004) Pittsburgh Post Gazette. Feb. 5, 2004: A-8.

Tseng, K.T., and Collicott, S.H. (2000) Fluidic Spray Control. ILASS Americas, 16th Annual Conference on Liquid Atomization and Spray Systems, Monterey, CA.

U.S. EPA (1983) Design Manual – Neutralization of Acid Mine Drainage. EPA-600/2 83-001. Washington, D.C.

Wehrli, B. (1990) Redox Reactions of Metals at Mineral Surfaces. In: Aquatic Chemical Kinetics: Reaction Rates of Processes in Natural Waters. W. Stumm, John Wiley & Sons, Inc., New York, NY.